

The northern termination of the Cache Creek terrane in Yukon: Middle Triassic arc activity and Jurassic–Cretaceous structural imbrication

Luke Bickerton, Maurice Colpron, H. Daniel Gibson, Derek Thorkelson, and James L. Crowley

Abstract: The northernmost part of the Cache Creek terrane lies in south-central Yukon and comprises metavolcanic rocks, hemipelagic chert and shale, newly identified volcanoclastic and clastic rocks (Michie formation, informal), pyroxenite and gabbro intrusive rocks with an arc to back-arc geochemical signature, as well as tectonized and serpentinized ultramafic rocks. The proximally sourced Michie formation yielded zircon from two samples with unimodal peaks at 245.85 ± 0.07 and 244.64 ± 0.08 Ma. These dates are likely close to the depositional ages and compare favourably with those from the Kutcho assemblage of northern British Columbia. The Michie formation is exposed along the northwestern flank of Mount Michie and represents singular detrital input from a nearby eroding island-arc. The Cache Creek terrane rocks are imbricated with epiclastic and carbonate rocks of the Stikinia and Lower Jurassic siliciclastic rocks of the synorogenic Whitehorse trough. This imbrication records two compressional deformation phases in the region: (1) an initial phase of west-verging thrusting along the Judas Mountain fault that placed the Cache Creek terrane rocks over the arc and basinal rocks of Stikinia and Whitehorse trough; and (2) a second phase of east-verging thrusting along the Mount Michie fault that repositioned rocks of Stikinia and the Whitehorse trough structurally above those of the Cache Creek terrane. Deformation in the centre of the study area was followed by emplacement of a coarse-grained syenite that yielded $^{40}\text{Ar}/^{39}\text{Ar}$ biotite and muscovite cooling ages of 165–160 Ma.

Key words: Cache Creek, Kutcho, Cordillera, terrane accretion, intra-oceanic arc.

Résumé : La partie la plus septentrionale du terrane de Cache Creek est située dans le centre sud du Yukon et renferme des roches métavolcaniques, des cherts et shales hémipélagiques, de roches volcanoclastiques et clastiques nouvellement découvertes (formation de Michie, nom informel), des roches intrusives pyroxénitiques et gabbroïques présentant une signature géochimique d'arc à arrière-arc, ainsi que des roches ultramafiques tectonisées et serpentinisées. Deux échantillons de la formation de Michie, de source proximale, ont produit des zircons qui ont donné des pics monomodaux à $245,85 \pm 0,07$ et $244,64 \pm 0,08$ Ma. Ces âges s'approchent vraisemblablement des âges de dépôt et ressemblent à ceux de l'assemblage de Kutcho du nord de la Colombie-Britannique. La formation de Michie est exposée le long du flanc nord-ouest du mont Michie et représente un unique apport de détritiques issus de l'érosion d'un arc insulaire situé à proximité. Les roches du terrane de Cache Creek sont imbriquées avec des roches épicastiques et carbonatées de la Stikinie et des roches silicoclastiques du Jurassique inférieur de la fosse synorogénique de Whitehorse. Cette imbrication témoigne de deux phases de déformation en compression dans la région, soit (1) une phase initiale de chevauchement vers l'ouest le long de la faille du mont Judas, qui a placé les roches du terrane de Cache Creek sur les roches d'arc et de bassin de la Stikinie et de la fosse de Whitehorse, et (2) une seconde phase de chevauchement vers l'est le long de la faille du mont Michie, qui a repositionné des roches de la Stikinie et de la fosse de Whitehorse structurellement au-dessus de celles du terrane de Cache Creek. La déformation dans le centre de la région à l'étude a été suivie de la mise en place d'une syénite grenue qui a produit des âges de refroidissement $^{40}\text{Ar}/^{39}\text{Ar}$ sur biotite et muscovite de 165–160 Ma. [Traduit par la Rédaction]

Mots-clés : Cache Creek, Kutcho, Cordillère, accréation de terranes, arc intraocéanique.

Introduction

The Mesozoic evolution of the western margin of North America involved a complex history of crustal growth by successive terrane accretions that resulted in development of the Cordilleran orogenic collage (e.g., Helwig 1974; Coney et al. 1980; Monger et al. 1982; Nokleberg et al. 2000; Nelson et al. 2013; Fig. 1, inset). Construction of the northern Cordilleran orogen began with the Early to Middle Jurassic accretion of the Intermontane terranes to the western margin of North America (e.g., Colpron et al. 2015).

The Intermontane terranes consist of mid-Paleozoic to early Mesozoic arc terranes (Yukon–Tanana, Stikinia, and Quesnellia) that developed in the peri-Laurentian realm (Nelson et al. 2013), and the Cache Creek terrane, which formed as an accretionary complex in the forearc region of Stikinia and Quesnellia (Fig. 1, inset; Monger and Nokleberg 1996; Struik et al. 2001). The Cache Creek terrane consists of fragments of oceanic crust, seamounts with limestone caps, arc crust, supra-subduction zone ophiolite, pelagic sedimentary rocks, and is overlain by synorogenic clastic

Fig. 1. Geology of the northern Cache Creek terrane; adapted from digital bedrock geology maps of the British Columbia Geological Survey (2015) and Yukon Geological Survey (2018). Inset shows location of the northern Cache Creek terrane within the Canadian Cordillera (after Colpron and Nelson 2011). Box inset northeast of Carcross indicates location of study area at the northern termination of the Cache Creek terrane shown in Fig. 2. Note location of (1) the type Kutcho assemblage (ca. 255–242 Ma; Childe and Thompson 1997; Schiarizza 2012) southeast of Dease Lake; (2) the Nakina area, south of Atlin, studied by English et al. (2010) and McGoldrick et al. (2017); and (3) a dated gabbro body (245.4 ± 0.8 Ma; Gordey et al. 1998), east of the study area. Abbreviations within oval inset: AX, Alexander terrane; CC, Cache Creek terrane; NAb, basal facies of western Laurentian margin (including Selwyn basin and Kootenay terrane); NAc, Laurentian autochthonous cover and craton; NAp, platformal facies of the western Laurentian margin (including Rocky and Mackenzie mountains); OK, Okanagan terrane; QN, Quesnellia; ST, Stikinia; Van., Vancouver; Wh., Whitehorse; WR, Wrangellia; YT, Yukon–Tanana terrane. [Colour online.]

rocks (Mihalynuk 1999; McGoldrick et al. 2017). Lower Permian (Cisuralian) limestone in the Cache Creek terrane contain fusulinid and conodont fauna of Tethyan affinity (Monger and Ross 1971; Orchard et al. 2001), which contrast with coeval McCloud fusulinid fauna in Quesnellia and Stikinia that indicates a peri-Laurentian affinity (e.g., Miller 1987; Belasky et al. 2002). This contrast in faunal affinities is an important component of tectonic models proposed for amalgamation of the Intermontane terranes (e.g., Wernicke and Klepacki 1988; Mihalynuk et al. 1994, 2004; Johnston and Borel 2007).

The Cache Creek terrane has been described as an accretionary or subduction complex in which diverse and disparate oceanic assemblages are juxtaposed (e.g., Struik et al. 2001; Golding 2018). Studies of the terrane in central British Columbia (southern Cache Creek; Fig. 1, inset) suggest that the Cache Creek complex comprises mainly plume-influenced oceanic crust (Tardy et al. 2001), including spreading-ridge and oceanic plateau imbricated with trench-fill sediments, carbonate atoll, and possible arc crust. Studies of the northern Cache Creek terrane in northern British Columbia (Fig. 1) indicate that significant components of the terrane comprise intra-oceanic arc crust and supra-subduction zone ophiolite juxtaposed with oceanic seamount, and pelagic and forearc sediments (Fig. 1; e.g., Mihalynuk 1999; English and Johnston 2005; Schiarizza 2012; Zagorevski et al. 2015; Zagorevski 2016; McGoldrick et al. 2017). The degree of heterogeneity between conodont faunas from different parts of the Cache Creek terrane suggests that they evolved independently until their Mesozoic accretion within the Intermontane terranes (Golding 2018).

In this paper, we describe the geological relationships of the Cache Creek terrane near Marsh Lake, Yukon (Fig. 2). Previously mapped at reconnaissance scale (Wheeler 1961), the terrane affinity of this area was enigmatic and never fully included in the Cache Creek terrane. We present new geochemical and geochronological data that support correlation with Early Triassic intra-oceanic arc successions documented in the Cache Creek terrane of northern British Columbia.

Regional geology

Stikinia and Quesnellia (Fig. 1, inset) are generally considered to have developed as a contiguous arc system because of their similarities in lithologies, Devonian to Early Jurassic age range, contact relationships, and geochemical and isotopic signatures (e.g., Souther 1977; Dostal et al. 1999). The oldest exposed rocks in both terranes are Paleozoic arc assemblages that are thought to correlate, in part, with the peri-Laurentian Yukon–Tanana terrane (Jackson et al. 1991; McClelland 1992; Mihalynuk et al. 1994; Nelson and Friedman 2004; Colpron et al. 2006; Nelson et al. 2006). Similarities in Quesnellia and Stikinia include correlation of prominent Upper Triassic augite-(plagioclase)-phyric volcanic rocks assigned to the Stuhini Group (Souther 1977; Monger et al. 1991) and Lewes River Group in northern Stikinia (Wheeler 1961; Hart 1997), and to the Nicola Group (Mortimer 1987), the Shonectaw Formation (Gabrielse 1998), and Semenof formation (informal, Tempelman-Kluit 1984, 2009; Simard 2003) in Quesnellia (Fig. 1). In addition to similar volcanic stratigraphy, a suite of Triassic to Early Jurassic plutons intrudes both Stikinia and Quesnellia, and merges at a northern apex within the Yukon–Tanana terrane

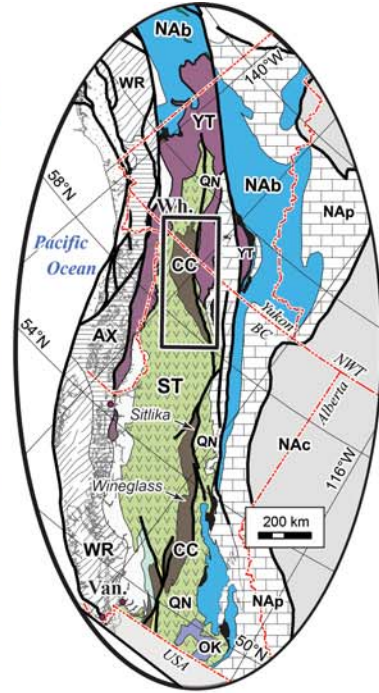
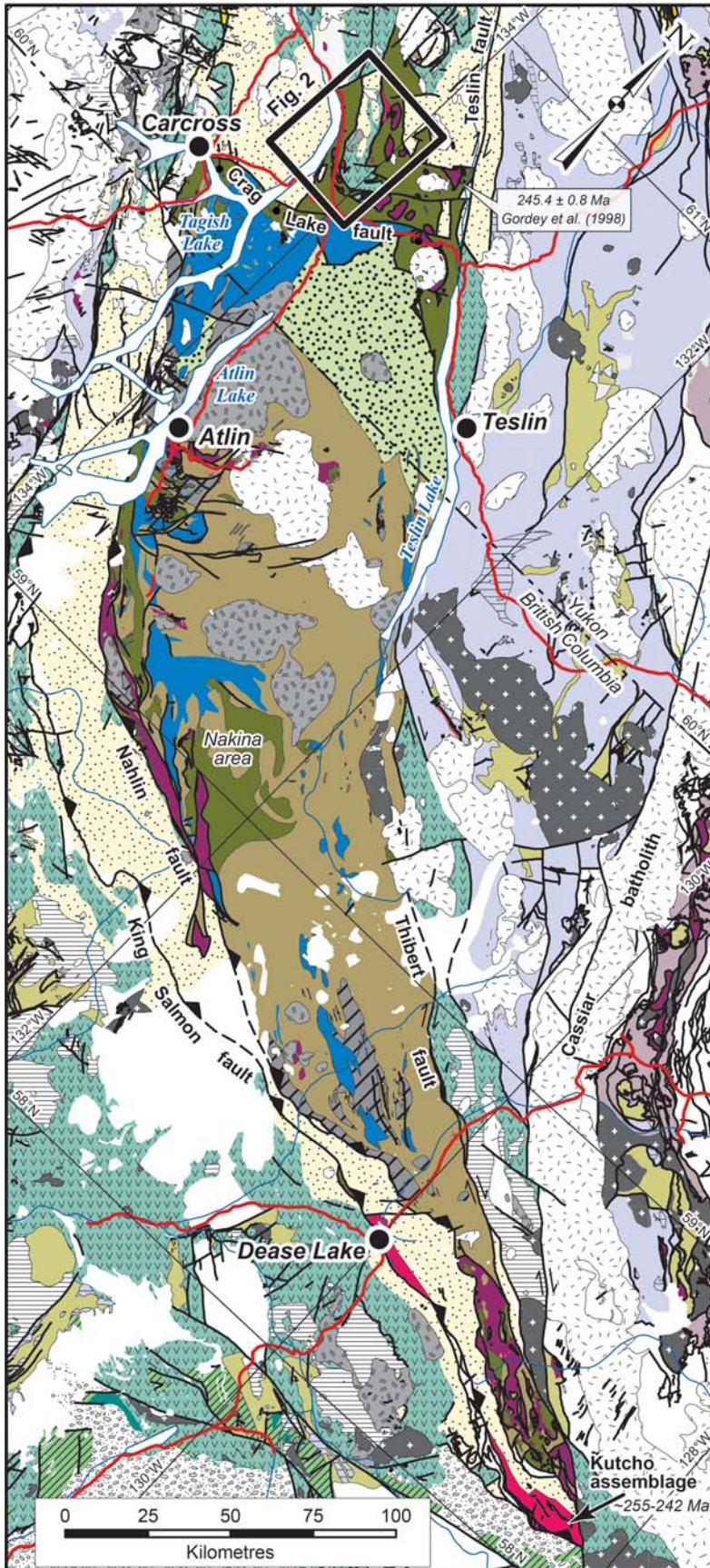
(Wheeler and McFeely 1991; Nelson et al. 2013). The geochemical and isotopic evidence connecting Stikinia and Quesnellia throughout the late Paleozoic and early Mesozoic include negative Nb anomalies, a similar juvenile $^{87}\text{Sr}/^{86}\text{Sr}$ signature, as well as positive epsilon (ϵ_{Nd}) values of 6–8 (Armstrong 1988; Dostal et al. 1999, 2009).

The Cache Creek terrane has a mixture of Mississippian to Jurassic lithologies in variable proportions that include components of oceanic crust consisting of ultramafic rocks, gabbro, basalt, ribbon chert, and massive limestone (e.g., Monger 1975; Gabrielse 1991; Struik et al. 2001). The age range of ultramafic rocks in the Cache Creek terrane is loosely constrained to be Permian to Triassic in central British Columbia (e.g., Struik et al. 2001), and Early Triassic in southern Yukon based on a single U–Pb zircon date of 245.4 ± 0.8 Ma (Gordey et al. 1998; Fig. 1). Intrusive rocks occur both as lozenges in mélangé and as undeformed bodies that have been dated in the Atlin area of British Columbia by U–Pb zircon at 261.4 ± 0.3 Ma (Devine 2002; Mihalynuk et al. 2003).

The Cache Creek terrane contains thick limestone with local occurrences of early Permian verbeekinitid fusulinid with distinctive Tethyan affinity (e.g., Monger and Ross 1971). The complex also includes sedimentary rocks such as greywacke, siltstone, and slate that are interpreted to be part of a forearc assemblage. The Kedahda formation (informal) of the Cache Creek terrane in northern British Columbia comprises argillite, fine-grained wacke, and radiolarian chert that range from Guadalupian (middle Permian) to Lower Jurassic in age (Cordey et al. 1991; Jackson 1992; Mihalynuk 1999). In the eastern part of the terrane, a mélangé locally contains Lower Jurassic blueschist (ca. 173 Ma Ar–Ar phengite cooling age, Mihalynuk et al. 2004). The presence of Permian limestone with exotic Tethyan fauna, in conjunction with the Lower Jurassic blueschist cooling age in the eastern part of the terrane, suggests there was protracted subduction of Panthalassic lithosphere beneath the Quesnellia–Stikinia arc in this timeframe that led to development of the Cache Creek accretionary complex.

The northern end of Cache Creek terrane extends from northern British Columbia to south-central Yukon where it terminates near Marsh Lake (Fig. 1). The Cache Creek terrane is overlapped and imbricated with the Lower to Middle Jurassic basal sedimentary rocks of the Whitehorse trough (Laberge Group). Clastic strata of the Whitehorse trough unconformably overlie the upper Paleozoic and lower Mesozoic rocks of Stikinia, Quesnellia, and Cache Creek terranes (e.g., White et al. 2012; Colpron et al. 2015). The basin is interpreted to record forearc deposition along the flank of the Stikinia–Quesnellia arc (Mihalynuk et al. 1994; English and Johnston 2005; Canil et al. 2006), which transitioned into a synorogenic piggy-back basin overlying the Intermontane terranes during the Early to Middle Jurassic (Fig. 1; White et al. 2012; Colpron et al. 2015). The main phase of subsidence and deposition in the Whitehorse trough ended in the Middle Jurassic; this is marked by the unconformably overlapping Upper Jurassic – Lower Cretaceous Tantalus Formation in Yukon that records deposition within intermontane fluvial and lacustrine settings (Long 2015).

Westward imbrication of the Cache Creek terrane with Stikinia and the Whitehorse trough in the northern Cordillera is documented



- Cretaceous pluton
 - Middle Jurassic pluton
 - Early Jurassic pluton
 - Late Triassic pluton
- Synorogenic basins**
- Bowser basin (M Jurassic - L Cretaceous)
 - Whitehorse trough (E-M Jurassic)
 - Late Triassic - Jurassic clastic rocks
- Cache Creek terrane**
- L-M Triassic volcanic/clastic rocks (Kutcho/Michie)
 - Pennsylvanian-Permian limestone (Teslin & Horsefeed)
 - Permian volcanic/clastic rocks (French Range)
 - Mississippian-Triassic chert-argillite (Kedahda)
 - Mississippian-Permian basalt (Nakina)
 - ultramafic complex
- Stikinia/Quesnellia**
- Lower to Middle Jurassic volcanic/clastic rocks (Hazelton)
 - Upper Triassic volcanic/clastic rocks (Stuhini/Lewes R./Takla/Semenof)
 - upper Paleozoic volc./sed. rocks (Stikine/Takhini/Klinkit/Fourmile)
- Yukon-Tanana terrane**
- mid-Paleozoic metasedimentary and metavolcanic rocks
 - mid-Paleozoic metaplutonic rocks
- Slide Mountain terrane**
- mid to upper Paleozoic basalt, chert, argillite
 - ultramafic complex

Fig. 2. Bedrock geology map of the Marsh Lake (after Bickerton 2014b). Inset shows poles to foliation measurements of D₁ (S₁) and D₂ (S₂) folds shown in equal area lower hemisphere plots; the S₂ plot also contains fold axis measurements attributed to D₂ folds. Rose petals in each inset plot represent vectors of foliation strike (using right-hand rule). Lines of section for Fig. 5 are provided. [Colour online.]

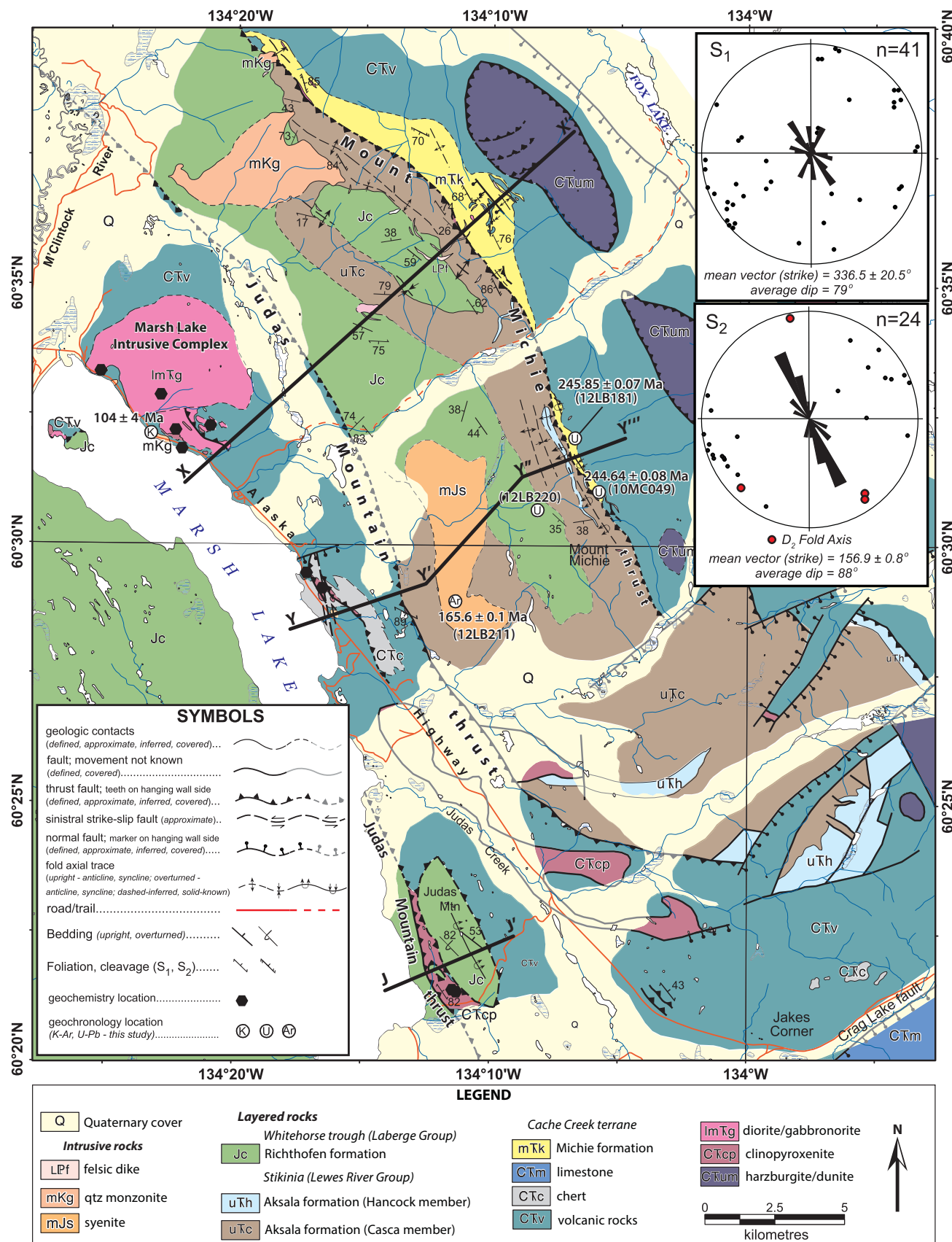
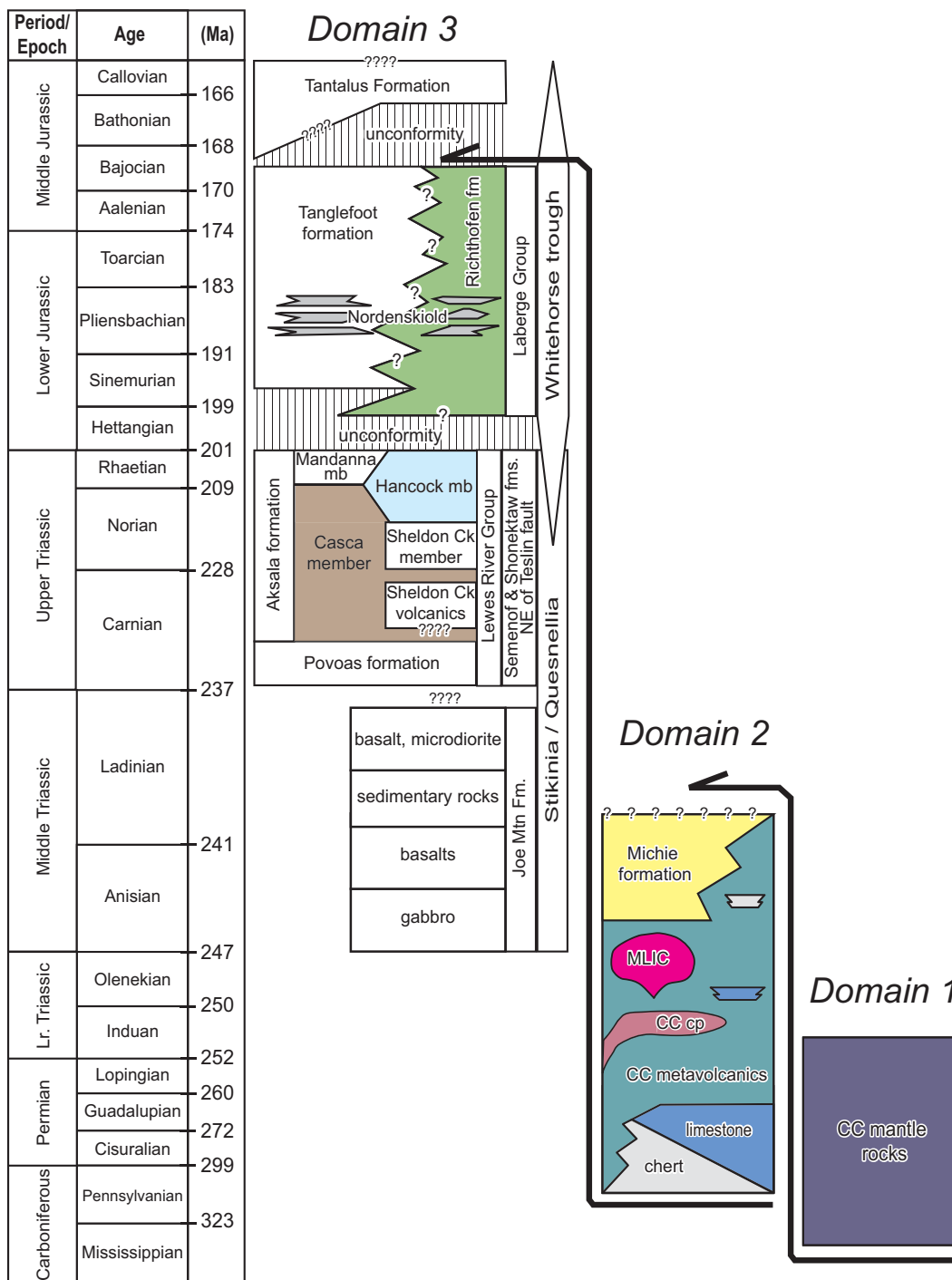


Fig. 3. Composite stratigraphic section for the Cache Creek terrane, Stikinia, and Whitehorse trough in southern Yukon (modified after [Hart 1997](#); [Lowey 2004](#); [White et al. 2012](#); [Colpron et al. 2015](#); [Bordet 2018](#)). The coloured units are those observed in the study area. CC, Cache Creek; cp, clinopyroxenite; MLIC, Marsh Lake intrusive complex. Tectonostratigraphic domains (described in text) are labelled in italics. Age boundary picks (Ma) from [Walker et al. \(2012\)](#). [Colour online.]



by southwest-verging folds and thrusts that placed the accretionary complex onto Stikinia by early Bajocian (ca. 175–171 Ma, [Mihalynuk et al. 2004](#); [Evenchick et al. 2001](#)). In northern British Columbia, the Nahlin fault is one of these thrusts, having brought Cache Creek rocks over strata of Whitehorse trough and Stikinia (Fig. 1; [Gabrielse 1991, 1998](#); [Mihalynuk 1999](#); [Mihalynuk et al. 2004](#); [Evenchick et al. 2005](#)). Evidence for juxtaposition of Cache Creek rocks structurally above the Whitehorse trough is preserved in the Tantalus Formation (Middle Jurassic), which re-

ceived chert clasts shed from the exhuming Cache Creek terrane ([Long 2005](#); Fig. 3). The imbrication and exhumation of the Cache Creek terrane also resulted in deposition into the Middle Jurassic – Lower Cretaceous synorogenic Bowser Basin in central British Columbia (e.g., [Ricketts et al. 1992](#); [Gabrielse 1998](#); [Shirmohammad et al. 2011](#)).

In the Dease Lake area, between the Nahlin and King Salmon faults, metabasalt and serpentinite occur as the structural base of the Cache Creek terrane and are spatially associated with Permo-

Triassic bimodal volcanic and volcanoclastic rocks of the Kutcho assemblage (Childe and Thompson 1997; Childe et al. 1998; Schiarizza 2011; Fig. 1). Schiarizza (2011) described the Kutcho assemblage as a juvenile oceanic arc sequence within the Cache Creek terrane that forms part of the basement to strata of the Whitehorse trough. The U–Pb zircon ages in felsic volcanic rocks within the Kutcho assemblage, ranging from 255.13 ± 0.96 to 242 ± 1 Ma (Childe and Thompson 1997; Schiarizza 2012), correlates with the volcanic Sitlika and Wineglass assemblages located along strike southwards in central British Columbia (e.g., Schiarizza 2013; Fig. 1 inset). This age correlation, and the similarities in lithologies and structural relationships at the western boundary of the Cache Creek terrane, led to the identification of an intra-oceanic arc complex termed the “Sitlika–Kutcho–Venables arc” (Logan and Mihalynuk 2014). The western boundary of the Cache Creek terrane traces north from the Kutcho assemblage along the Nahlin fault (Fig. 1; e.g., Mihalynuk 1999) and extends to the Carcross area in southern Yukon, where it is apparently cut by the northeast-striking Crag Lake fault (Hart and Radloff 1990). The trace of this crosscutting fault relationship is partially obscured by the intrusion of post-accretionary mid- to Late Cretaceous granitoid rocks (Hart 1995). The most northerly rocks assigned to the Cache Creek terrane extend north of the Crag Lake fault in the Marsh Lake area (Fig. 2); these rocks are described below.

The northern termination of the Cache Creek terrane

At surface, the northern termination of the Cache Creek terrane, near Marsh Lake in southern Yukon, is structurally imbricated with carbonate and clastic rocks of the Lewes River (Stikinia) and Laberge (Whitehorse trough) groups (Figs. 1 and 2). In this area, the Cache Creek terrane comprises five main lithological assemblages: (1) metavolcanic rocks, (2) hemipelagic chert and shale, (3) volcanoclastic and clastic rocks, (4) pyroxenite and gabbro intrusive rocks, and (5) tectonized and serpentinitized ultramafic rocks (Figs. 2 and 3; Bickerton 2014a, 2014b). The units are described below and ordered by tectonostratigraphic domain (see Fig. 3), from the highest interpreted thrust panel to the lowest; this order also describes the rocks from oldest to youngest in the succession.

Domain 1: Cache Creek terrane ultramafic rocks

Near Marsh Lake, in the eastern part of the study area, ultramafic rocks of the Cache Creek terrane are characterized by a composition of harzburgite to dunite and typically form larger exposures within thrust sheets structurally above all other units (Figs. 2 and 3).

The large harzburgite–dunite bodies in the eastern part of the study area (Fig. 2) are coarse grained, contain abundant magnetite, and have veins of antigorite and chrysotile throughout. Locally, the harzburgite shows a subtle cumulate texture of olivine with interstitial orthopyroxene. These rocks also occur as rounded blocks in a sheared serpentinite matrix that has been extensively carbonatized. The ultramafic bodies are in fault contact with volcanic rocks of the Cache Creek terrane, but unlike those in the western part of the map area, carbonate \pm Cr mica alteration is not a prominent feature near these contacts.

Domain 2: Cache Creek terrane sedimentary and mafic volcanic/intrusive rocks

Chert

Chert is a dominant lithology of the Cache Creek terrane in British Columbia (Monger 1975; Gabrielse, 1991), but is less extensive at its northern termination in Yukon (Figs. 1–3). In the eastern part of the study area, massive to ribbon chert with rare limestone is locally intercalated with the metavolcanic rocks. The chert is grey to reddish brown in colour and locally contorted by soft-

sediment deformation structures (Fig. 4c). Chert beds are 5–10 cm thick and are interbedded with 1–3 cm horizons of argillite. Chert also occurs as subordinate lenses within the metavolcanic rocks and as clasts in volcanic breccia.

Metavolcanic rocks

Mafic to intermediate metavolcanic rocks are the dominant lithologies in the Cache Creek terrane of the Marsh Lake area (Figs. 2, 3, and 4a), ranging from dark grey basaltic to light grey andesitic compositions. The rock is typically massive, mainly composed of fine- to medium-grained plagioclase and clinopyroxene within an aphanitic chloritic matrix. The metavolcanic rocks locally show pillows (e.g., Fig. 4b), amygdules, and hyaloclastic textures, and can contain decimetre- to metre-scale lenses of limestone and chert. In the western part of the map area (Fig. 2), the metavolcanic rocks are locally crosscut by subvolcanic gabbro and clinopyroxenite bodies as determined by field observations. Typical clinopyroxenites in the western part of the map area (near Judas Mountain and Judas Creek) are spatially associated with the Marsh Lake gabbroic intrusive complex, locally intruding volcanic rocks and chert of the Cache Creek terrane, and occur near planar structures, where they are altered to carbonate \pm Cr-mica in fault contact with clastic sedimentary rocks of the Laberge Group (Whitehorse trough; Fig. 2).

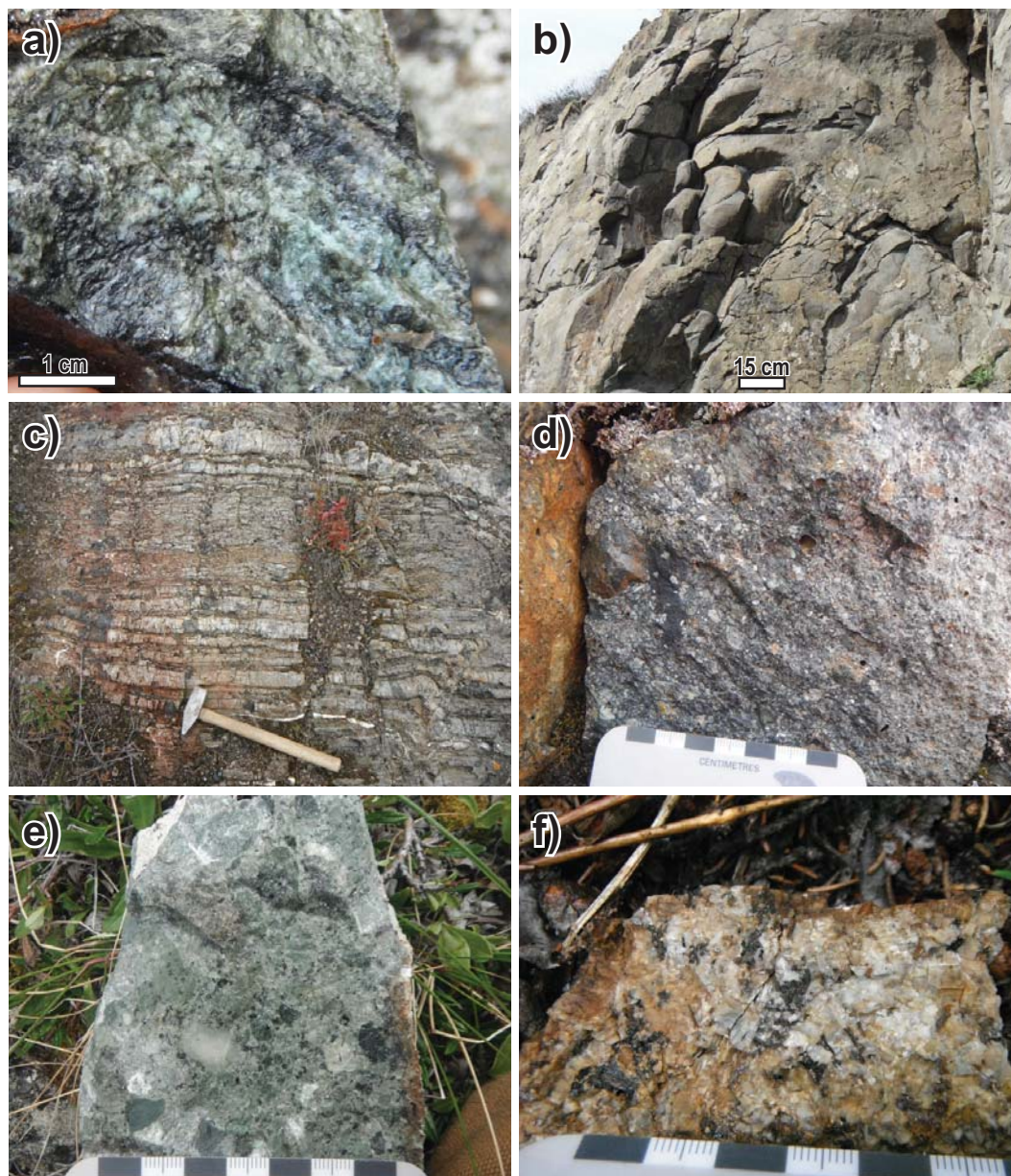
In the eastern part of the map area, the andesite and basalt are intercalated with green to grey volcanoclastic sandstone, particularly in proximity to the gradational contact with the newly recognized and overlying Michie formation (informal), described below.

Volcanoclastic and clastic rocks of the Michie formation (new unit)

The Michie formation is a newly proposed informal stratigraphic unit composed of a previously undocumented clastic unit that is in gradational contact with underlying mafic metavolcanic rocks in the footwall of the Mount Michie thrust (Fig. 3). There is no complete section of Michie formation in the study area because the upper part of the unit is everywhere truncated by the Mount Michie thrust, but the unit is approximately at least 500 m thick. The succession consists mainly of medium- to coarse-grained, immature, volcanoclastic to polyimictic sandstone and wacke (e.g., Fig. 4d), but also includes pebble orthoconglomerate and dark grey siltstone. For approximately 15 km along the north–northwest flanking ridge to Mount Michie, the formation is discontinuously exposed with variable thickness for each defined lithology (Fig. 2); thus, this area is defined as the composite-stratotype section for the newly identified unit. The thickest section of sandstone and wacke (approximately 200 m thick) occurs approximately 2 km north–northwest from Mount Michie. Southwest of Fox Lake, approximately 11 km north–northwest of Mount Michie, the sandstone–wacke thins to centimetre- to metre-scale beds within a fining-upward sequence of volcanoclastic orthoconglomerate – sandstone – carbonaceous siltstone (locally interbedded with buff-weathering limestone beds) that is irregularly brecciated in a matrix of intermediate volcanic rocks.

The sandstone varies from calc-lithic to volcanic-lithic sandstone, with subrounded grains and moderate to poor sorting. The conglomerate comprises subrounded to angular clasts of mafic and felsic volcanic rocks, fine-grained mafic intrusive clasts, limestone, chert, and very-fine-grained siltstone. Siltstone is commonly coupled with sandstone beds in 1–2 m (thickness) intervals, with sandstone grading into siltstone. Locally, siltstone forms massive sections with up to 250 m apparent thickness. Petrographic analysis of eight sandstone samples from the Michie formation utilizing the Gazzi-Dickinson point-counting method (Dickinson 1970; Ingersoll 1978; Ingersoll et al. 1984) shows a predominance of volcanic lithic clasts suggesting provenance from

Fig. 4. (a) Light green mafic metavolcanic rocks of the Cache Creek terrane (CCT) with fine-grained plagioclase, clinopyroxene in chloritic to serpentized matrix. (b) Highway outcrop of pillowed basalt in the CCT. (c) Outcrop of ribbon chert of the CCT in the Marsh Lake area. (d) Fresh surface of Michie formation immature volcanoclastic rocks containing clasts of mafic and felsic volcanic rocks and fine-grained mafic intrusive with minor limestone, chert, and siltstone. (e) Fresh surface of matrix-supported conglomerate of Laberge Group. (f) Fresh surface of coarse-grained to pegmatitic syenite from centre of the Marsh Lake map area (Fig. 2). [Colour online.]



an undissected arc source (Fig. 5; Tables 1 and Supplementary Table S1¹).

Marsh Lake intrusive complex

A gabbroic complex crops out near the north end of Marsh Lake (Fig. 2). It intrudes exclusively mafic volcanic rocks of the Cache Creek terrane as a set of intrusive lenses with a shallow (<20°) northeast dip. The Marsh Lake intrusive complex comprises medium- to coarse-grained to porphyritic hornblende diorite to gabbro and, locally, to clinopyroxenite. These rocks are intensely foliated and altered to chlorite and epidote. Although samples were collected for mineral separation, no zircon or baddeleyite were ob-

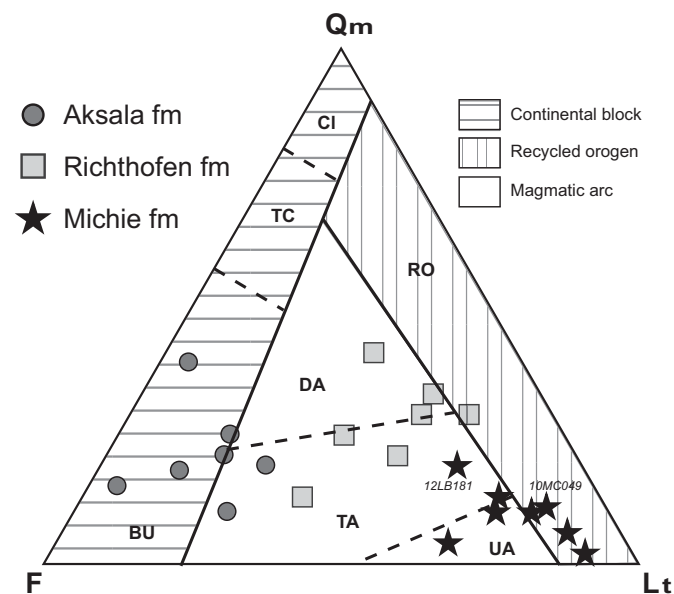
tained for U-Pb geochronology. Ophitic plagioclase-bearing gabbroic rocks locally grade into augite-dominant clinopyroxenite. Clinopyroxene is subhedral to euhedral, and typically has embayment and sieve textures, as well as local cumulate textures. Olivine-phyric diabase dikes crosscut these rocks throughout the Marsh Lake intrusive complex with no preferred orientation.

Domain 3: Stikinia and Whitehorse trough rocks

Stikinia (Lewes River Group)

Regionally, the Lewes River Group (Late Triassic; Lees 1934; Wheeler 1961) comprises volcanic rocks of the Povoas formation

Fig. 5. Ternary quartz(monocrystalline)–feldspar–lithic clast (QmFLt) plot. Plotted points represent spread of compositions from formations of the Stikine terrane (Aksala fm), Whitehorse trough (Richthofen fm), and the Cache Creek terrane (new Michie formation). The provenance fields of Dickinson et al. (1983) are indicated and specific domains abbreviated: BU, basement uplift; CI, craton interior; DA, dissected arc; RO, recycled orogenic; TA, transitional arc; TC, transitional continental; UA, undissected arc. The degree of arc dissection increases from right to left in the arc-related provenance fields (UA, TA, DA).



and overlying sedimentary rocks of the Aksala formation (both informal units of Tempelman-Kluit 1984, 2009). The Aksala formation includes three members of epiclastic and carbonate rocks, two of which, the Casca and Hancock members, are represented in the Marsh Lake area (Figs. 2 and 3). The Carnian-Norian Casca member includes strata that vary from black-grey, moderately to well-sorted, submature, subangular coarse-grained arkosic arenite (Fig. 5; Tables 1 and Supplementary Table S1¹), to fine-grained, thinly laminated, dark grey argillaceous siltstone. The Hancock member conformably overlies the Casca member and is a massive, crystalline, locally fossiliferous light-grey limestone that is mainly exposed at the south end of the Marsh Lake area. Microfossils and ammonoids from Hancock limestone in this area indicate a mid-upper Norian age for these strata (Wheeler 1961; Gordey and Stevens 1994; Colpron 2011; Bickerton 2014b).

Whitehorse trough: Laberge Group (Richthofen formation)

The Lower to Middle Jurassic Richthofen formation (informal) includes black turbiditic siltstone, greenish-grey sandstone, and thick horizons of matrix-supported polymictic conglomerate (Wheeler 1961; Hart 1997; Lowey et al. 2009). It is exposed in the centre of the study area, where it unconformably overlies the Casca member, and along the shore of Marsh Lake near Judas Mountain (Fig. 2). The medium- to coarse-grained sandstone typically forms beds 5–15 cm thick coupled with fine-grained, green-brown mudstone beds 3–5 cm thick. The sandstone is a fine- to coarse-grained, subangular, and compositionally immature feldspathic litharenite. The sandstone framework is dominated by sedimentary and volcanic lithic fragments, but also contains quartz and feldspar as major components (Fig. 5; Tables 1 and Supplementary Table S1¹), and hornblende as a minor component. The black limestone forms monotonous strata up to 1200 m thick. The conglomerate contains pebbles to boulders of limestone, very-fine-grained grey siltstone, felsic plutonic, and less commonly, felsic

volcanic lithologies, supported by a volcanoclastic sandstone matrix (Fig. 4e).

Post-accretionary intrusive rocks

A number of post-accretionary granitoid plutons and numerous rhyodacite dikes intrude rocks of the Cache Creek terrane, Stikinia and Whitehorse trough near Marsh Lake. Of these, the largest exposed body is a pluton of syenitic composition that intruded rocks of the Casca member and Richthofen formation in the centre of the map area, west of Mount Michie (Fig. 2). The syenite is coarse grained to pegmatitic, dominated by alkali-feldspar, and contains small (5–10 mm) books of coarse-grained biotite and muscovite that are partially altered to chlorite and sericite, respectively (Fig. 4f). The pluton is poorly exposed and contact relationships with major structures are uncertain, although sedimentary strata of the Laberge and Lewes River groups are hornfelsed near the syenite. This syenite pluton was also originally considered part of the mid-Cretaceous Whitehorse plutonic suite (e.g., Gordey and Makepeace 2001), but ⁴⁰Ar/³⁹Ar data presented below indicates an older Middle Jurassic age.

A majority of the post-accretionary intrusions, however, range in composition from granodiorite to hornblende quartz monzonite and have been assigned to the mid-Cretaceous Whitehorse plutonic suite (Wheeler 1961; Gordey and Makepeace 2001; Colpron 2011; Colpron et al. 2016) based on textural and mineralogical similarities to a coarse-grained diorite stock exposed along the eastern shore of Marsh Lake (Fig. 2) with a single K–Ar date of 104 ± 4 Ma (Hart 1995). The granodiorite to hornblende quartz monzonite intrusions are mostly coarse grained and equigranular with variable alteration. The largest body occurs in the northern part of the map area where it intrudes both Casca member and Richthofen formation (Fig. 2). Near the northern edge of the map area, a small quartz monzonite pluton crosscuts the Mount Michie thrust, which juxtaposes sedimentary rocks of Stikinia and Whitehorse trough in its hanging wall against the Michie formation (Cache Creek terrane) in its footwall (see below; Fig. 2), thereby placing a potential younger limit on timing of faulting in the area.

Rhyodacite dikes are assumed to be the youngest rocks in the Marsh Lake area as they are undeformed, apart from magmatic flow-banding near dike margins, and can crosscut all units at various localities. The dikes are typically 1–2 m wide and composed of medium-grained, spherulitic, quartz and feldspar-phyric rhyolite to dacite. Regionally, these volumetrically small set of dikes are assigned a late Paleocene age (Fig. 2) due to their similar intermediate character to the Paleocene-aged Sifton range volcanic rocks (e.g., Miskovic and Francis 2004) and Mount Skukum intrusive rocks (e.g., Love et al. 1998) to the northwest, and to the Eocene Sloko Group volcanic rocks to the southwest (e.g., Souther 1991; Mihalynuk 1999).

Structure

Due to limited exposure throughout much of the map area, major structural features are inferred primarily from map patterns, bedding–cleavage relationships, and changes in foliation intensity. The structural style of the Marsh Lake area is dominated by two sets of folds and related cleavages, and two major thrust systems (Figs. 2 and 6). Outcrop-scale folds are typically open and upright (Fig. 7a) but become tighter and steeply inclined near major faults (Fig. 7b) with variable intensity of cleavage development. S₁ is a tightly spaced (typically <5 cm) fracture cleavage with an average orientation of 337/79°NE (Fig. 2 inset) that is best preserved in sedimentary strata of the Laberge and Lewes River groups. S₂ is a widely spaced (~5–10 cm) parallel fracture cleavage with an average orientation of 157/88°SW (Fig. 2 inset) that is likely lower temperature than S₁ as it is strongly developed near the traces of D₂ thrusts (e.g., Mount Michie thrust, see below) where it overprints D₁ structures (Fig. 7c). The D₂-related fold axes (Fig. 2,

Fig. 6. Structural cross sections for the Marsh Lake area; lines of section and legend are shown in Fig. 2. Black pins present the apparent strike (filled circle, representing in and out of section) and dip (line, representing dip direction) of bedding in sedimentary rocks at surface for the cross section. [Colour online.]

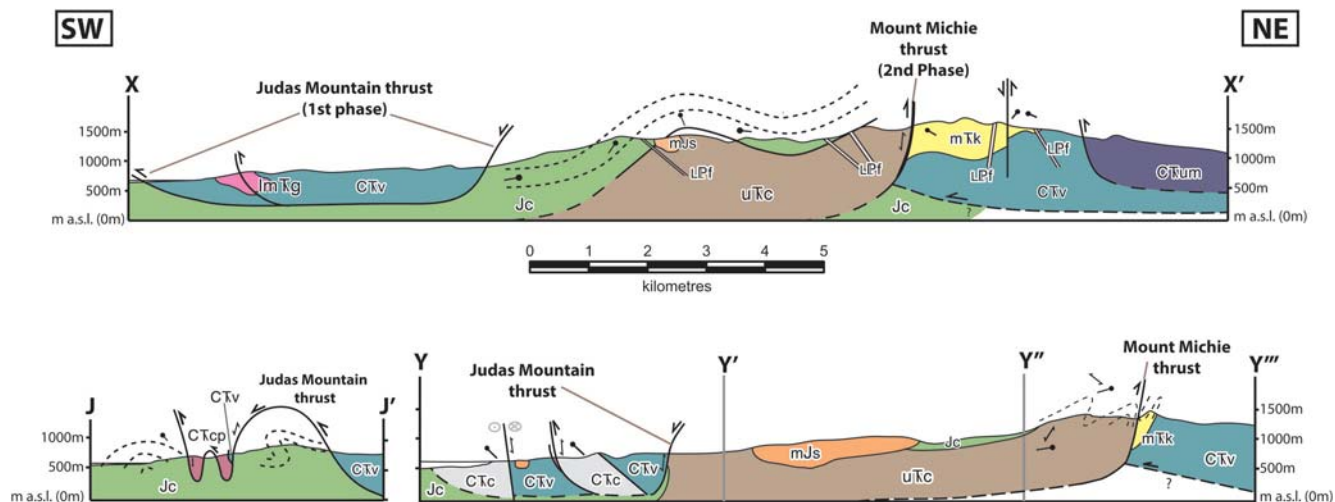


Table 1. Summary of point-counting for sandstones of the Marsh Lake area.

Formation	QFL%			LmLvLs%			Fr%			
	Q	F	L	Lm	Lv	Ls	Bt	D	M	
Richthofen										
Mean	35.08	27.76	37.16	0.00	83.66	16.34	1.03	10.79	1.37	
SD	10.44	12.43	4.70	0.00	5.18	5.18	0.54	5.83	1.45	
Aksala										
Mean	31.06	62.16	6.78	0.00	66.75	33.25	1.93	7.10	5.32	
SD	9.34	9.47	5.87	0.00	23.64	23.64	1.35	4.50	3.26	
Michie										
Mean	16.81	15.85	67.34	4.46	78.82	16.73	9.54	2.80	6.71	
SD	6.54	7.44	8.08	7.95	12.65	6.61	5.34	2.25	5.31	
Formation	QmFLt%			QmPK%			QpLvmLsm%			
	Qm	F	Lt	Qm	P	K	Qp	Lvm	Lsm	P/F
Richthofen										
Mean	27.29	27.76	44.95	76.67	23.33	0.00	16.41	69.99	13.59	0.93
SD	8.94	12.43	8.17	25.88	25.88	0.00	7.36	8.25	4.06	0.07
Aksala										
Mean	21.00	62.16	16.84	44.48	48.99	6.54	60.10	25.07	14.83	0.86
SD	9.22	9.47	9.12	30.48	27.09	6.44	28.24	15.62	15.66	0.07
Michie										
Mean	9.26	15.85	74.89	93.38	6.50	0.12	10.47	71.84	18.45	0.98
SD	5.55	7.44	9.89	18.72	18.37	0.35	8.49	15.07	8.89	0.02

Note: Mean measures average number of points counted in all samples for a given formation, SD measures the standard deviation for the counts. Detrital modes (found in Supplementary Table S1¹) have been recalculated to 100 per cent basis for each mineral assemblage, with heavy minerals separated as per cent of total fragments (Fr%). Q, total quartz; Qm, monocrystalline quartz; Qp, polycrystalline quartz; F, total feldspar; K, potassium feldspar; P, plagioclase; Lm, metamorphic lithics; Lv, volcanic lithics; Ls, sedimentary lithics; Lvm, volcanic and metamorphic lithics; Lsm, sedimentary and metamorphic lithics; Lt, unstable lithic fragments (Lv + Ls); Lt, total lithic fragments (L + Qp); Bt, biotite; D, dense minerals (hornblende, pyroxene, opaques); M, phyllosilicates (biotite, chlorite, muscovite).

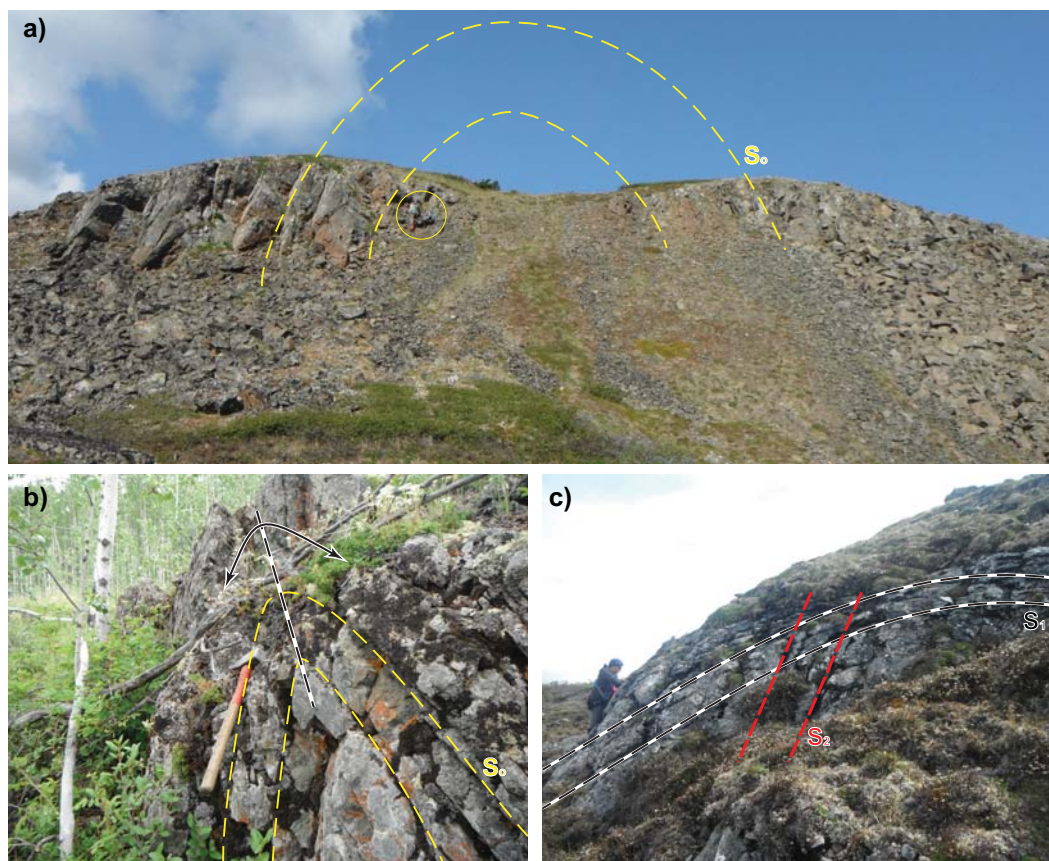
inset) suggest the folds are northwest–southeast trending and have a subhorizontal plunge. Both sets of foliations lack new mineral growth.

The Judas Mountain thrust (D_1) juxtaposes rocks of the Cache Creek terrane in its hanging wall over those of the Whitehorse trough in its footwall (Figs. 2 and 6). The thrust is exposed near the southern shore of Marsh Lake, east of Judas Mountain, where footwall rocks of the Laberge Group are deformed by tight folds overturned to the southwest that are inferred to be fault-related D_1 folds that reflect thrust vergence. At this location, the hanging wall of the Judas Mountain thrust comprises mafic and ultramafic rocks of the Cache Creek terrane, including foliated carbonate/Cr-mica altered pyroxenite and serpentinite, and extensive hydrothermal veining. The thrust strikes northwest and dips mod-

erately to steeply to the northeast and is inferred to project northwesterly beneath Marsh Lake. The thrust resurfaces on the island at the north end of Marsh Lake, where the strike is deflected to the southwest (Fig. 2).

Map relationships suggest that the Judas Mountain thrust is folded (Figs. 2 and 6). Judas Mountain itself is underlain by a fester of Laberge Group surrounded by mafic and ultramafic rocks of the Cache Creek terrane. East of the Alaska Highway, the steeply-southwest-dipping contact between Cache Creek metavolcanic rocks and sedimentary rocks of the Lewes River and Laberge groups is inferred to represent the folded surface of the Judas Mountain thrust (Fig. 2). Alternatively, this contact could be a younger, out-of-sequence fault juxtaposing younger over older rocks. At higher structural level, the thrust faults juxtaposing

Fig. 7. (a) Broad open folds of Michie formation approximately 900 m east of the Michie fault; geologist for scale. (b) Outcrop-scale west-verging folding in the Judas Mountain area of Laberge Group sedimentary rocks; hammer for scale. (c) D_2 overprint on D_1 in Whitehorse trough sedimentary rocks, north of Mount Michie. Sandstone shows foliation S_1 (shallow fabric) that is folded and crosscut by S_2 (steeply dipping to west–southwest foliation); geologist for scale. [Colour online.]



harzburgite/dunite bodies with metavolcanic rocks of the Cache Creek terrane in the eastern portion of the map area (Figs. 2 and 6) are also inferred to have developed during D_1 southwest-verging contraction.

The Mount Michie thrust (D_2) is a south–southeast striking, steeply-southwest-dipping reverse fault that juxtaposes rocks of the Whitehorse trough (Laberge Group) and Stikinia (Casca member), which occupy the footwall of the D_1 Judas Mountain thrust, over the Michie formation and Cache Creek metavolcanic rocks to the east (Figs. 2 and 6). Near the fault, the S_2 spaced fracture cleavage crosscuts D_1 folds and cleavage (Fig. 7c). Development of the Mount Michie thrust is associated with northeast-verging folds that are characterized by an anticline in the hanging wall, and a syncline in the footwall to the Mount Michie thrust (e.g., section Y''–Y''' of Fig. 6), further indicating reverse movement along this fault.

Litho geochemistry of Cache Creek mafic igneous rocks

Analytical methods

Results are presented for whole-rock geochemical analysis of 16 mafic rock samples from the Cache Creek terrane. These include nine representative samples collected from gabbroic intrusive and mafic volcanic rocks of the Cache Creek terrane, as determined and named in the field, as part of this study (Table 2; units assigned based on mapping, Fig. 2). Major and trace elements were analyzed at Activation Laboratories (Actlabs) in Ancaster, Ontario, using whole-rock lithium metaborate/tetraborate fusion ICP and ICP-MS (inductively coupled plasma mass spec-

trometry). Fused samples were diluted and analyzed by Perkin Elmer Sciex ELAN 6000 ICP-MS, with three blanks and five controls (three before sample group and two after) analyzed with the sample group. Duplicates were fused and analyzed every 15 samples and the instrument was recalibrated every 40 samples. An external standard (MRG-1, Mount Royal gabbro) was included twice with the sample batch (one before and one after unknown samples) for quality control purposes. The resultant data were combined with unpublished data for seven samples from the same area collected by S.J. Piercey in 2005 (herein termed “SJP samples”; Table 2). Details of the analytical methods, precision, and accuracy for the SJP samples are presented in Ruks et al. (2006) and Piercey et al. (2004).

Results

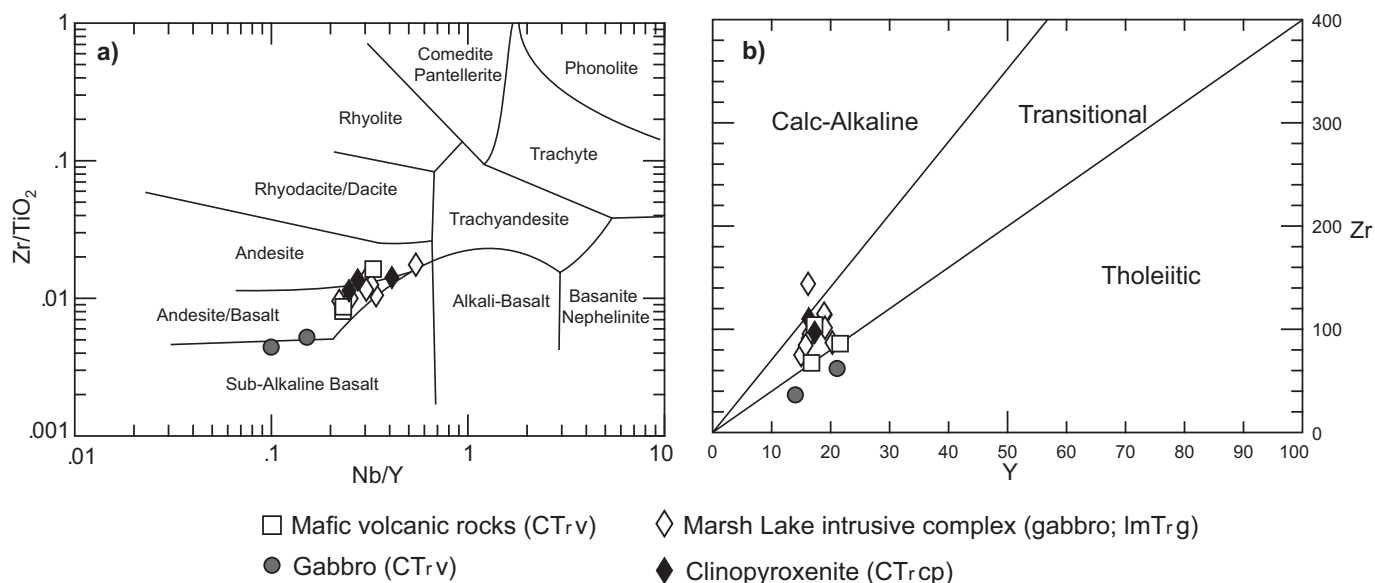
Most samples have minor to extensive saussuritization and serpenitization of the original clinopyroxene and plagioclase-rich phases. Although the least altered samples were collected for analysis, we assume the abundance of some major and trace elements may not be representative of the original whole-rock chemistry. Accordingly, major element weight percentages were recalculated to a volatile-free (anhydrous) basis. After recalculation, the SiO_2 concentrations in the mafic samples range from 48.94 to 60.75 wt %, MgO from 2.79 to 10.09 wt %, and TiO_2 from 0.64 to 1.21 wt % (Table 2). Our interpretations below are primarily derived from the least mobile high-field-strength and rare earth elements to minimize the influence of alteration similar to previous studies that dealt with low-grade metamorphic alteration (e.g., Gibson et al. 1982).

Table 2. Whole-rock major and minor element and rare earth element abundances for mafic rocks in the map area.

Sample Lithology	12LB020 Gabbro	12LB056 Gabbro	12LB217 Pyroxenite	11LB024 Gabbro	05SJP065-1-1 Gabbro	11LB033 Gabbro	05SJP078-1-1 Gabbro	11LB036 Pyroxenite	11LB029 Pyroxenite	11LB036 Pyroxenite	11LB026 Mafic volcanic	05SJP065-2-1(1) Mafic volcanic	05SJP074-1-1 Mafic volcanic	05SJP067-1-1 Gabbro	11LB027 Gabbro	
Unit	lmTrg	lmTrg	lmTrg	lmTrg	lmTrg	lmTrg	lmTrg	CfTrcp	CfTrcp	CfTrcp	rock CfTrv	rock CfTrv	rock CfTrv	CfTrv	CfTrv	
SiO ₂	50.27	53.34	53.14	53.37	56.39	51.07	50.62	48.94	52.11	51.65	60.75	51.94	49.53	57.50	50.39	50.72
Al ₂ O ₃	17.18	15.38	17.30	17.39	17.43	15.87	15.82	16.82	13.01	11.67	16.77	16.81	11.28	17.94	17.88	14.20
Fe ₂ O ₃ (T)	9.82	9.67	9.11	9.82	7.27	10.18	10.69	10.88	8.77	10.06	7.49	10.38	9.60	7.71	9.21	11.31
MnO	0.17	0.17	0.16	0.19	0.13	0.17	0.19	0.18	0.14	0.16	0.12	0.19	0.18	0.15	0.15	0.17
MgO	4.36	5.75	4.69	4.21	3.28	5.46	5.47	5.74	9.46	7.48	2.79	5.24	10.09	3.13	6.74	7.43
CaO	10.69	7.71	7.95	6.19	6.19	9.46	9.46	10.07	10.87	11.43	5.48	7.98	14.39	9.96	6.56	11.72
Na ₂ O	3.24	3.19	3.72	3.41	4.40	3.79	2.63	1.86	2.19	1.90	4.03	3.59	1.86	3.53	3.67	2.83
K ₂ O	3.10	3.54	2.92	3.04	3.69	2.63	3.94	4.34	2.18	3.78	1.55	2.47	2.02	2.51	1.03	0.30
TiO ₂	0.72	0.91	0.75	0.85	0.73	0.96	0.76	0.73	0.86	0.84	0.78	1.07	0.78	1.21	0.82	0.78
P ₂ O ₅	0.46	0.35	0.28	0.35	0.41	0.39	0.42	0.43	0.42	1.02	0.25	0.32	0.28	0.32	0.14	0.11
LOI	4.26	2.77	2.77	3.42	4.27	3.15	2.09	2.86	10.28	2.94	3.11	3.95	2.18	2.86	2.29	3.76
Total*	98.49	100.70	98.79	99.06	99.36	99.67	99.61	100.07	99.35	99.76	97.91	99.70	100.04	99.93	99.30	99.90
Cs	0.6	4.8	2.1	3		4	0.2	0.6	0.6	0.6	0.6	3.7	0.6	0.6	0.3	0.3
Rb	53	79	67	72	72	50	78	92	41	33	32	45	38	50	24	5
Sr	418	675	1210	873	888	793	867	682	1528	244	601	852	676	656	268	140
Ba	1705	2973	2540	2589	>1400	1365	>1400	>1400	3293	1308	1101	2971	1326	>1400	220	362
Sc	24	36	28	29	12	22	22	22	32	39	17	37	43	13	24	42
V	237	267	249	263	191	255	240	244	201	261	176	309	235	158	261	298
Cr	30	130	50	20	21	49	45	58	180	40	40	30	165	17	158	290
Ni	<20	<20	<20	<20	<1	9	5	11	90	40	<20	<20	29	6	55	60
Cu	130	120	100	70	61	77	90	95	60	120	10	100	59	22	85	150
Zn	80	90	90	84	84	84	89	86	60	80	100	110	70	90	63	80
Mo	<2	<2	<2	<2	<2	<2	<2	86	<2	<2	<2	<2	<2	<2	<2	<2
W	<0.5	0.9	<0.5	0.8	<10	<10	<10	<10	0.6	<0.5	0.6	0.7	<10	<10	<10	<0.5
Sn	1	2	1	1		1			1	2	1	2				<1
As	5	<5	<5	5		<5			<5	<5	<5	<5				<5
Tl	0.38	0.37	0.47	0.39		0.47			0.23	0.23	<0.05	0.33				<0.05
Bi	<0.1	<0.1	<0.1	<0.1		<0.1			0.1	0.1	<0.1	<0.1				<0.1
U	3.62	2.67	2.99	3.12	4.25	3.17	3.08	2.97	1.85	2.12	1.4	1.81	2.00	2.98	0.16	0.14
Th	7.63	5.42	5.73	7.39	10.03	7.28	7.33	6.92	4.9	5.08	3.94	4.95	4.62	5.99	0.30	0.41
Pb	20	12	15	20		9			9	19	10	13				<5
Hf	2.3	2.2	2	2.7	3.70	2.60	2.40	2.20	2.5	3	2.8	2.2	1.90	2.70	1.10	1.7
Zr	91	87	75	114	144.0	101.4	95.4	84.4	97	115	110	86	67.4	104.1	36.4	63
Ta	0.3	0.29	0.23	0.27		0.22			0.22	0.27	0.4	0.21				0.2
Nb	5	4.5	3.8	5.7	8.8	6.5	5.3	4.8	4.3	5.2	6.7	5	3.9	5.7	1.4	3.2
Y	16.3	20.3	15	19	16.18	19.05	16.43	15.76	17.3	18.9	16.3	21.6	16.76	17.29	14.02	21.1
La	27.1	19	20	26.4	33.22	26.07	25.33	24.22	27.7	20.9	18.7	23.6	17.04	20.39	3.03	4.36
Ce	51.6	38.8	38.2	50.6	69.4	48.85	47.61	45.17	59.5	45.1	37.8	47.4	32.14	37.23	7.54	11.4
Pr	5.58	4.29	4.24	5.8	6.90	5.94	5.77	5.50	7.21	5.75	4.43	5.76	4.01	4.36	1.18	1.64
Nd	22.7	18.2	17.5	22.9	27.32	24.12	23.40	22.44	30.2	24.2	17.7	22.9	16.87	16.97	5.90	8.19
Sm	4.79	4.3	3.72	4.88	5.37	5.09	4.98	4.70	5.99	5.41	3.85	4.77	3.95	3.59	1.86	2.6
Eu	1.33	1.25	1.08	1.22	1.53	1.50	1.45	1.38	1.52	1.52	1.03	1.39	1.14	1.11	0.73	0.885
Gd	4.37	4.47	3.6	4.42	4.56	4.56	4.30	4.05	4.6	4.84	3.36	4.27	3.79	3.40	2.40	3.1
Tb	0.59	0.67	0.52	0.61	0.57	0.63	0.58	0.56	0.64	0.71	0.54	0.68	0.54	0.51	0.41	0.59
Dy	3.11	3.61	2.78	3.3	3.20	3.71	3.27	3.13	3.33	3.46	3.05	3.63	3.24	3.21	2.62	3.64
Ho	0.6	0.74	0.55	0.66	0.59	0.73	0.64	0.61	0.64	0.65	0.6	0.72	0.65	0.67	0.55	0.75
Er	1.67	2.15	1.61	1.84	1.65	2.03	1.76	1.69	1.68	1.76	1.66	2.13	1.81	1.96	1.60	2.16
Tm	0.244	0.301	0.23	0.268	0.23	0.29	0.25	0.24	0.236	0.235	0.232	0.295	0.26	0.29	0.23	0.313
Yb	1.63	2.07	1.53	1.78	1.55	1.90	1.60	1.54	1.48	1.56	1.56	1.91	1.74	1.99	1.52	2.02
Lu	0.268	0.345	0.259	0.283	0.227	0.277	0.235	0.225	0.236	0.241	0.254	0.314	0.253	0.301	0.229	0.324

*Major elements recalculated to a volatile free basis, but loss on ignition (LOI) and total weight % presented as original (before recalculation) values.

Fig. 8. (a) Zr/TiO₂ vs. Nb/Y rock classification diagram of Winchester and Floyd (1977). All Cache Creek samples from Marsh Lake area plot in the subalkaline field. (b) Zr–Y diagram of Barrett and MacLean (1999); most samples plot in the transitional field.



On the Zr/TiO₂ vs. Nb/Y classification diagram of Winchester and Floyd (1977), our Cache Creek samples plot in the subalkaline field and range from basaltic andesite to subalkaline basalt (Fig. 8a). On the calc-alkaline/tholeiitic basalt series differentiation diagram of Barrett and MacLean (1999; Fig. 8b), most samples from the Cache Creek terrane are transitional between tholeiitic and calc-alkaline compositions. On mid-ocean ridge basalt (MORB)-normalized multi-element plots (Figs. 9a–9b), the Cache Creek mafic rocks show enrichment in the more immobile, incompatible elements Th, Ta, Nb, and Zr that are slightly higher than an average calc-alkaline basalt pattern. Chondrite-normalized rare earth elements plots show (La/Lu)_n ratios ranging from 5.9 to 15.7, slightly higher than the average ocean island basalt (OIB; Figs. 9c–9d). Two samples of metagabbro collected outside the Marsh Lake intrusive complex show a (La/Lu)_n of 1.4, slightly depleted in light rare earth elements compared with the average enriched-type MORB (Fig. 9d). The heavy rare earth element profiles are relatively flat ((Gd/Lu)_n of 1.2–2.5) for all samples (Figs. 9c–9d).

The light rare earth element enriched samples from the Marsh Lake area also have high ratios of Th/Nb (0.59–1.5) and Ce/Nb (5.6–13.8). On the Th–Zr–Nb discriminant diagram of Wood (1980; Fig. 10a), all Marsh Lake samples plot in the arc field. The enrichment of Th and Nb relative to Yb further suggests the rocks have an enriched mantle source relative to typical arc magmas (Pearce and Peate 1995; Fig. 10b). Two samples collected outside the Marsh Lake intrusive complex and interpreted in the field as metagabbro (05JJP067-1-1 and 11LB027; Table 2) plot closer to typical mantle values (Figs. 9b, 10a, and 10b) and may indicate that the arc rocks were built upon a substrate of back-arc to MORB affinity with an enriched mantle source.

Comparison with other data from the Cache Creek terrane

The Cache Creek terrane is commonly described as an oceanic assemblage on account of its dominant lithologic association of chert, argillite, basalt, and ultramafic rocks (e.g., Monger 1975; Mihalyuk 1999; Struik et al. 2001). Local carbonate buildups and affiliated basalt are generally interpreted as oceanic seamounts that were incorporated into the accretionary complex.

In its type area in southern British Columbia, mafic volcanic rocks of the southern Cache Creek terrane are dominantly OIB with minor normal-type MORB basalt (Tardy et al. 2001; Fig. 10). This led Lapierre et al. (2003) to conclude that much of the oceanic

crust preserved in the Cache Creek accretionary complex was influenced by a plume and represent relic of oceanic seamount and (or) plateaux too buoyant to be subducted.

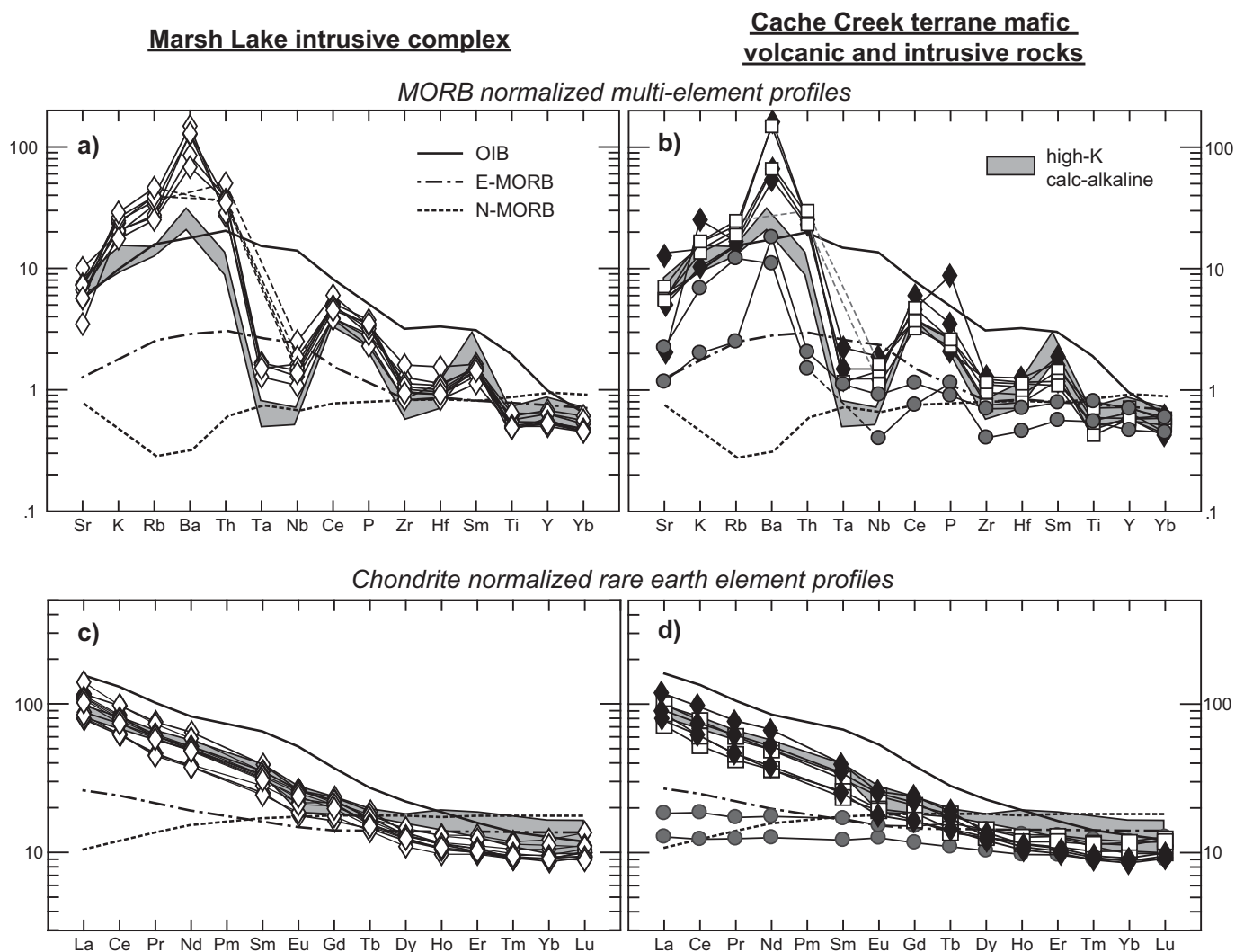
In contrast, mafic volcanic rocks in the northern Cache Creek terrane have geochemical affinities ranging from OIB to island-arc tholeiite, calc-alkaline basalt, back-arc basin basalt, and enriched-type MORB (English et al. 2010; Nakina area in Fig. 1). Rocks with OIB signatures are typically associated with carbonate (“carbonate assemblage” of English 2004; English et al. 2010; Fig. 10) and interpreted as seamounts, in agreement with the interpretation for the southern Cache Creek (Lapierre et al. 2003). However, English et al. (2010; their figs. 1 and 7) grouped all subalkaline compositions in the Nakina area under the “oceanic crustal assemblage”, and interpreted arc and back-arc origins for most mafic igneous rocks in the northern Cache Creek terrane.

Our data from the northern termination of the Cache Creek terrane in Yukon show predominantly calc-alkaline compositions for mafic volcanic and intrusive rocks, both from the Marsh Lake intrusive complex and for the intrusive to subvolcanic gabbros within the mapped Cache Creek terrane metavolcanic unit (e.g., unit CTrcp), suggesting these satellite intrusions are cogenetic with the Marsh Lake intrusive complex (Figs. 9 and 10). The geochemical signature of the mafic volcanic and intrusive rocks are consistent with an arc influenced by an enriched mantle source. Our data corroborates the conclusion of English et al. (2010) that much of the mafic rocks in the northern Cache Creek terrane represent intra-oceanic arc crust incorporated in the accretionary complex.

Geochronology

Three samples of coarse-grained sandstone were analyzed for detrital zircon U–Pb geochronology at Boise State University to constrain the maximum depositional age and provenance of clastic rocks in the Cache Creek terrane and Whitehorse trough. Two samples were collected from the Michie formation (12LB181 and 10MC049) of the Cache Creek terrane, in the footwall of the Mount Michie thrust (Fig. 2). The third sample is a sandstone from the Richthofen formation (Laberge Group; 12LB220) in the hanging wall of the Mount Michie thrust (Fig. 2). Data for the Richthofen sample were previously published as part of a regional provenance study of the Laberge Group (Colpron et al. 2015); it is repli-

Fig. 9. (a–b) Mid-ocean ridge basalt (MORB) normalized multi-element profiles for (a) gabbros of the Marsh Lake intrusive complex and (b) mafic volcanic rocks of the Cache Creek terrane. MORB normalizing values from Pearce (1983) and legend for these samples are shown in Figs. 9c and 9d. (c–d) Chondrite-normalized rare earth element profiles for (c) gabbros of the Marsh Lake intrusive complex and (d) mafic volcanic rocks of the Cache Creek terrane. Chondrite normalizing values, typical ocean island basalt and enriched-type MORB values from Sun and McDonough (1989). Typical high-K calc-alkalic basalt values from Gill (1981). Legend for samples from this study is same as shown in Fig. 8.



cated here for purpose of comparison with the new data from the Michie formation.

In addition to detrital zircon data, we also report here the results of $^{40}\text{Ar}/^{39}\text{Ar}$ analyses for micas from the syenite pluton located in the centre of our map area (Fig. 2). The $^{40}\text{Ar}/^{39}\text{Ar}$ analyses were performed by M. Heizler at New Mexico Geochronology Research Laboratory.

U–Pb methods

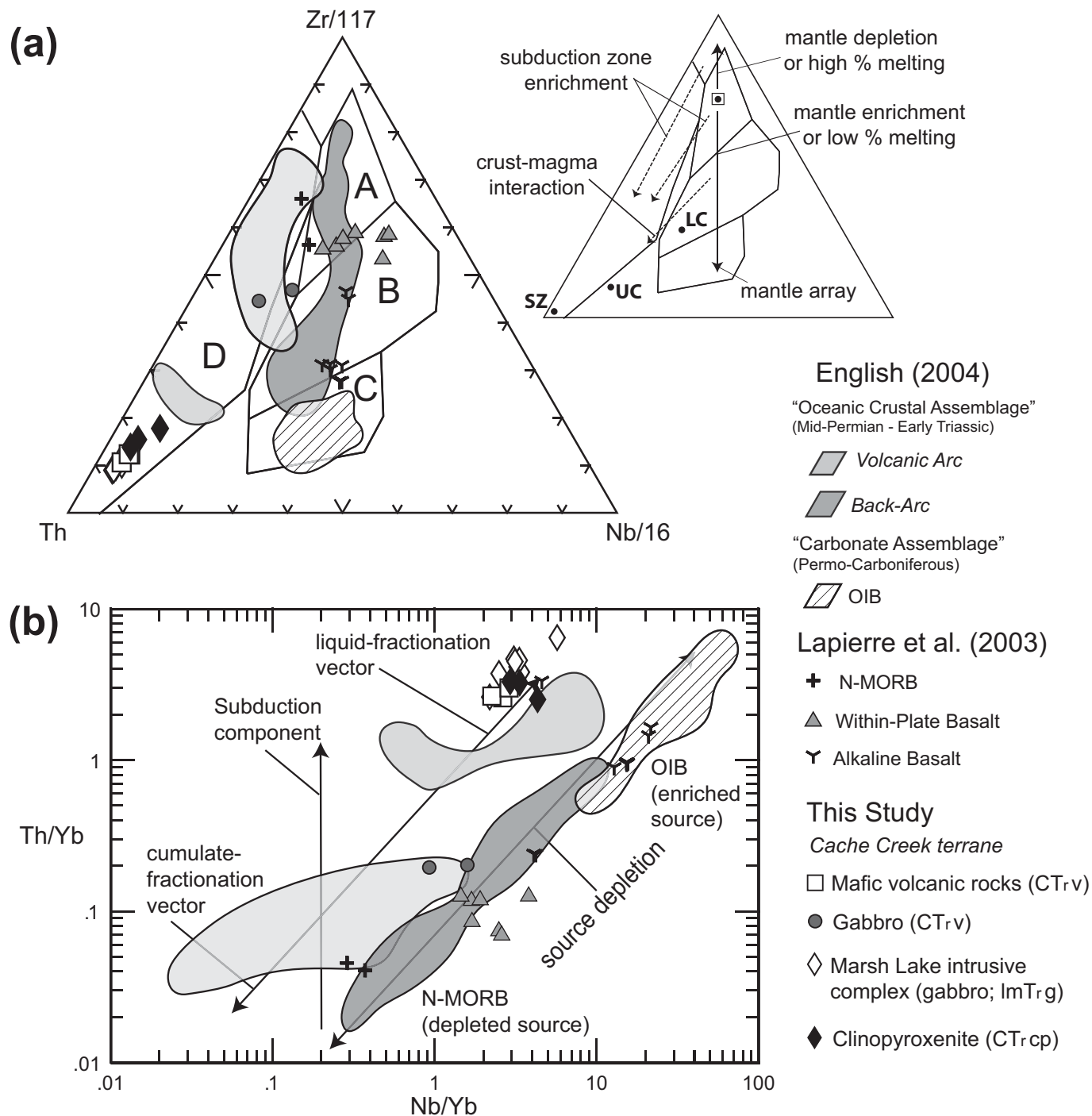
Detrital zircon U–Pb geochronology was undertaken at Boise State University using both the laser ablation inductively coupled plasma mass spectrometry (LA-ICPMS) and chemical abrasion isotope dilution thermal ionization mass spectrometry (CA-TIMS) methods.

LA-ICPMS

Zircon grains from two sandstone samples (10MC049 and 12LB220) were acquired using standard separation techniques and annealed at 900 °C for 60 h in a muffle furnace. They were mounted in epoxy, polished to the grain centres, and imaged using cathodoluminescence (CL) on a JEOL JSM-1300 scanning electron mi-

croscope to characterize the internal zoning of the zircon grains. The LA-ICPMS analyses were undertaken using a ThermoElectron X-Series II quadrupole ICPMS and New Wave Research UP-213 Nd:YAG UV (213 nm) laser ablation system. Data were collected from two samples during two analytical sessions conducted in May 2011 (session 1, sample 10MC049) and March 2013 (session 2, sample 12LB220). Laser ablation spot size was 25 μm , and a laser firing repetition rate of 10 Hz. Standard calibration uncertainties for $^{207}\text{Pb}/^{206}\text{Pb}$ dates are 0.7% and 0.5% (2σ) for experiments 1 and 2, respectively. Standard calibration uncertainty for $^{206}\text{Pb}/^{238}\text{U}$ dates are 2.0% and 3.2% (2σ for experiments 1 and 2, respectively). Errors on the $^{207}\text{Pb}/^{206}\text{Pb}$ and $^{206}\text{Pb}/^{238}\text{U}$ dates from individual LA-ICPMS analyses are given at 2σ , as are the errors on the weighted mean dates. A complete summary of the in-house analytical protocols, standard materials, and data reduction software used for acquisition and calibration of U–Pb dates and acquisition of a suite of high-field-strength elements and rare earth elements are provided by Bickerton (2014a). Analytical results for both samples are presented in Supplementary Table S2¹. As all zircon collected have

Fig. 10. (a) Tectonic discrimination diagram of Wood (1980), showing tectonic settings as fields within ternary. Field abbreviations: A, normal-type mid-ocean ridge basalt (MORB); B, enriched-type MORB and tholeiitic within-plate basalt (WPB) and differentiates; C, alkaline WPB and differentiates; D, destructive plate margin basalts and differentiates. Inset figure shows average basalt compositions from a subduction zone (SZ), upper crust (UC), lower crust (LC), and normal-type MORB (square). (b) Th/Yb vs. Nb/Yb diagram of Pearce and Peate (1995). Rocks of the Cache Creek terrane in the northern Cordillera generally show influence of subduction zone and enriched mantle sources (English 2004; English et al. 2010; this study). Rocks of the Cache Creek terrane in the central Cordillera generally plot close to the mantle array (projected between MORB and OIB) and are interpreted to have been derived in a within-plate environment (Lapierre et al. 2003).



ages that are Paleozoic or younger, the age interpretations are based on the $^{206}\text{Pb}/^{238}\text{U}$ chronometer.

CA-TIMS

Zircon grains extracted from the samples using standard separation techniques were mounted in epoxy and polished to

grain centres. Prior to CA-TIMS analyses, CL images were obtained. Approximately 8–10 zircon grains or fragments of grains from two samples of the Michie formation (10MC049, 12LB181) were selected for dating based on the CL images. The grains selected for analysis were removed from the epoxy mounts and were analyzed using a modified version of the

Table 3. U–Pb isotopic chemical abrasion isotope dilution thermal ionization mass spectrometry data.

Sample ^a	Radiogenic isotope ratios										Isotopic ages								
	²⁰⁶ Pb/ ²³⁸ U	mol % ²⁰⁶ Pb/ ²⁰⁶ Pb ^c	Pb*/ Pb _c ^c (pg)	²⁰⁶ Pb/ ²⁰⁴ Pb ^d	²⁰⁸ Pb/ ²⁰⁶ Pb ^e	²⁰⁷ Pb/ ²⁰⁶ Pb ^e	²⁰⁷ Pb/ ²³⁵ U ^e	% err ^f	²⁰⁶ Pb/ ²³⁸ U ^e	% err ^f	Corr. coef.	²⁰⁷ Pb/ ²⁰⁶ Pb ^g	±f	²⁰⁷ Pb/ ²³⁵ U ^g	±f	²⁰⁶ Pb/ ²³⁸ U ^g	±f		
12LB181																			
Z1	0.453	99.42%	51	3094	0.144	0.0511	0.222	0.2737	0.269	0.0389	0.077	0.699	243.97	5.12	245.67	0.59	245.85	0.19	
Z2	0.415	98.89%	26	1630	0.132	0.0510	0.322	0.2735	0.374	0.0389	0.084	0.687	241.71	7.42	245.52	0.82	245.92	0.20	
Z3	0.436	99.35%	45	2793	0.138	0.0511	0.206	0.2743	0.261	0.0389	0.079	0.778	247.43	4.73	246.10	0.57	245.96	0.19	
Z4	0.419	99.19%	36	2221	0.133	0.0513	0.270	0.2747	0.330	0.0389	0.077	0.817	252.81	6.22	246.43	0.72	245.76	0.19	
Z5	0.476	98.27%	17	1045	0.151	0.0512	0.445	0.2746	0.503	0.0389	0.097	0.662	250.88	10.23	246.35	1.10	245.87	0.23	
Z6	0.449	99.52%	61	3741	0.142	0.0511	0.184	0.2740	0.232	0.0388	0.074	0.742	247.31	4.24	245.85	0.51	245.70	0.18	
Z7	0.513	99.62%	79	4770	0.163	0.0512	0.141	0.2745	0.194	0.0389	0.073	0.818	249.93	3.24	246.26	0.42	245.87	0.18	
Z8	0.507	99.52%	62	3736	0.161	0.0512	0.146	0.2743	0.200	0.0389	0.071	0.832	248.62	3.37	246.16	0.44	245.91	0.17	
10MC049																			
Z1	0.630	99.61%	80	4660	0.200	0.0511	0.155	0.2731	0.210	0.0388	0.074	0.819	244.59	3.58	245.18	0.46	245.24	0.18	
Z2	0.627	99.65%	88	5104	0.199	0.0511	0.145	0.2728	0.201	0.0387	0.072	0.848	247.39	3.35	244.93	0.44	244.67	0.17	
Z3	0.604	98.82%	26	1527	0.192	0.0514	0.426	0.2746	0.485	0.0388	0.094	0.681	257.03	9.80	246.37	1.06	245.25	0.23	
Z4	0.653	99.22%	40	2303	0.207	0.0511	0.412	0.2731	0.463	0.0388	0.080	0.688	246.06	9.48	245.19	1.01	245.10	0.19	
Z5	0.667	99.38%	51	2928	0.212	0.0511	0.242	0.2722	0.292	0.0387	0.079	0.713	243.61	5.58	244.49	0.63	244.58	0.19	
Z6	0.713	99.64%	78	4422	0.226	0.0512	0.153	0.2732	0.205	0.0387	0.074	0.794	248.38	3.52	245.22	0.45	244.89	0.18	
Z7	0.769	99.52%	67	3745	0.244	0.0511	0.168	0.2725	0.215	0.0387	0.072	0.755	245.04	3.87	244.72	0.47	244.69	0.17	
Z8	0.696	99.05%	33	1890	0.221	0.0512	0.241	0.2736	0.290	0.0388	0.079	0.705	249.30	5.54	245.53	0.63	245.14	0.19	
Z9	0.515	2.3123	161	9648	0.163	0.0511	0.095	0.2724	0.155	0.0387	0.073	0.896	246.22	2.19	244.63	0.34	244.47	0.18	
Z10	0.656	0.7393	60	3484	0.208	0.0512	0.181	0.2730	0.235	0.0387	0.079	0.780	247.80	4.16	245.06	0.51	244.78	0.19	

^aZ1, Z2, etc., are analyses of single zircon grains annealed and chemically abraded (Mattinson 2005). Boldface type indicates analysis used in weighted mean calculation.

^bModel Th/U ratio calculated from radiogenic ²⁰⁸Pb/²⁰⁶Pb ratio and ²⁰⁷Pb/²³⁵U date.

^cPb* and Pb_c are radiogenic and common Pb, respectively. mol % ²⁰⁶Pb* is with respect to radiogenic and blank Pb.

^dMeasured ratio corrected for spike and fractionation only. Fractionation correction is 0.18 ± 0.03 (1 sigma) %amu (atomic mass unit) for single-collector Daly analyses, based on analysis of EARTHTIME ²⁰²Pb–²⁰⁵Pb tracer solution.

^eCorrected for fractionation, spike, common Pb, and initial disequilibrium in ²³⁰Th/²³⁸U. Common Pb is assigned to procedural blank with composition of ²⁰⁶Pb/²⁰⁴Pb = 18.042% ± 0.61%; ²⁰⁷Pb/²⁰⁴Pb = 15.537% ± 0.52%; ²⁰⁸Pb/²⁰⁴Pb = 37.686% ± 0.63% (1 sigma). ²⁰⁶Pb/²³⁸U and ²⁰⁷Pb/²⁰⁶Pb ratios corrected for initial disequilibrium in ²³⁰Th/²³⁸U using Th/U (magma) = 3.0 ± 0.3.

^fErrors are 2 sigma, propagated using algorithms of Schmitz and Schoene (2007) and Crowley et al. (2007).

^gDecay constants used based on Jaffey et al. (1971). ²⁰⁶Pb/²³⁸U and ²⁰⁷Pb/²⁰⁶Pb dates corrected for initial disequilibrium in ²³⁰Th/²³⁸U using Th/U (magma) = 3.0 ± 0.3.

chemical abrasion method of Mattinson (2005); a complete summary of the CA-TIMS method used in this study is provided by Bickerton (2014a).

Age interpretations based on the weighted mean $^{206}\text{Pb}/^{238}\text{U}$ ages were calculated using Isoplot 3.0 (Ludwig 2003; Table 3). Errors given at the 2σ confidence interval on the weighted mean age reflect the internal errors based on analytical uncertainties only, including counting statistics, subtraction of tracer solution, and blank and initial common Pb subtraction. Errors on the $^{206}\text{Pb}/^{238}\text{U}$ dates from individual grains are also given at the 2σ confidence interval. Results of the CA-TIMS analyses are presented in Table 3; analyses used in the weighted mean age calculation are indicated by boldface type.

$^{40}\text{Ar}/^{39}\text{Ar}$ methods

Micas from the syenite pluton, sample 12LB211, were separated by crushing the sample and hand-picking individual grains. Samples were loaded into machined Al discs and irradiated for 8 h in the central thimble at the United States Geological Survey reactor (Denver, Colorado, USA). Fish Canyon Tuff sanidine (FC-2) was used as neutron flux monitor with an assigned age of 28.201 Ma (Kuiper et al. 2008). Irradiated samples were analyzed for ^{40}Ar , ^{39}Ar , ^{38}Ar , ^{37}Ar , and ^{36}Ar at the New Mexico Geochronology Research Laboratory by M. Heizler. Details of instrumentation, analytical parameters, and argon data are presented in Supplementary Table S3¹.

U–Pb results

Michie formation

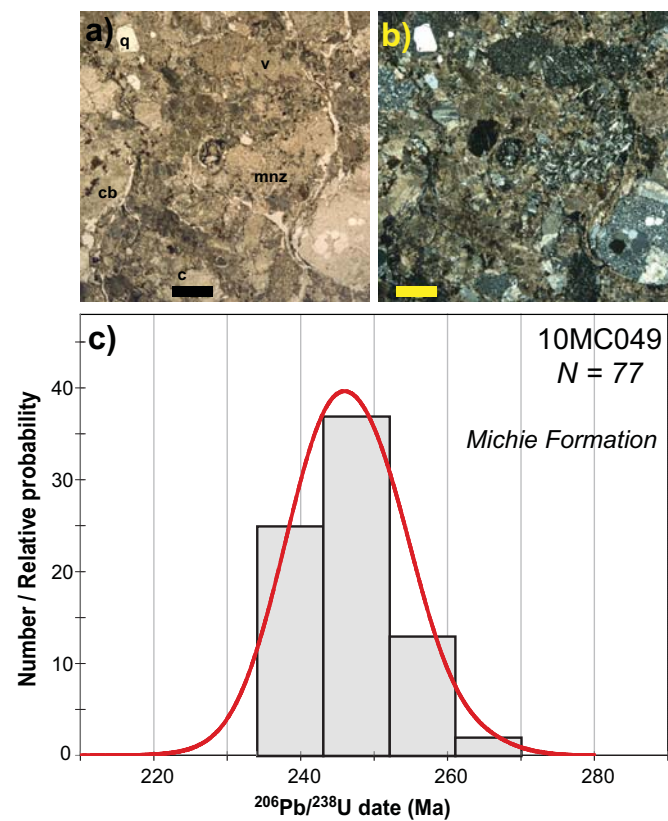
Sample 10MC049 is a coarse-grained calc-litharenite collected approximately 1 km north of Mount Michie (Fig. 2). Clasts in the sandstone are predominantly carbonate (55%), but also include up to 43% igneous clasts; mainly basalt to andesite, but also including monzonite and granodiorite grains (Figs. 11a and 11b; Bickerton 2014a). Seventy-seven zircon grains analyzed by LA-ICPMS yielded a narrow range of dates from 263 ± 10 to 235 ± 12 Ma, with a peak at ca. 245 Ma (Supplementary Table S2¹; Fig. 11c). In CL images, zircons from sample 10MC049 show uniform oscillatory zoning and sharply faceted morphologies, typical of detrital zircon from an igneous source that was proximal (Fig. 12a). To further constrain the age of the igneous source, 10 grains were analyzed by CA-TIMS. The five youngest zircon grains yielded equivalent concordant dates with a weighted mean of 244.64 ± 0.08 Ma (mean square weighted deviation = 1.7; Fig. 12b). The other five grains yielded older dates ranging from 244.89 ± 0.18 to 245.25 ± 0.23 Ma (Table 3).

Sample 12LB181 is a poorly sorted, immature, coarse-grained volcanic litharenite collected approximately 3.2 km north of Mount Michie (Fig. 2). The sandstone comprises both mafic and felsic volcanic grains, as well as minor chert and felsic plutonic clasts. It yielded only a few detrital zircon grains that show similar morphologies and zoning patterns in CL images as zircons in sample 10MC049 (Fig. 12c). Based on these similarities, eight zircon grains from 12LB181 were directly analyzed by CA-TIMS (Table 3). They yielded equivalent concordant $^{206}\text{Pb}/^{238}\text{U}$ dates with a weighted mean of 245.85 ± 0.07 Ma (mean square weighted deviation = 1.5; Fig. 12d). Results from both samples of the Michie formation suggest derivation from proximal ca. 245 Ma igneous sources, and likely closely reflect their depositional age as well.

Richthofen formation

Sample 12LB220 is a well-sorted, coarse-grained arkosic sandstone from a graded sandstone–siltstone succession in the Richthofen formation along the western ridge of Mount Michie (Fig. 2). There the sandstone is primarily composed of feldspar (85%), volcanic lithic fragments (10%), and only minor quartz (Bickerton 2014a). Sixty-nine zircon grains analyzed by LA-ICPMS (Supplementary Table S2¹) yielded dates ranging from 336 ± 24 to $181 \pm$

Fig. 11. (a) Transmitted-light photomicrograph of sample 10MC049 (scale bar = 1 mm). q, quartz; cb, carbonate clast; c, chert clast; v, volcanic clast (basalt/andesite); mnz, monzonite clast. (b) Crossed-nichols photomicrograph of sample observed in Fig. 11a. (c) Histogram and relative probability plot for detrital zircon $^{206}\text{Pb}/^{238}\text{U}$ dates from sample 10MC049 (plotted with Isoplot 3.0, Ludwig 2003). See Fig. 12a for example cathodoluminescence images for zircon grains. Bin width in the histograms is the average error on the dates. N, number of grains analyzed. [Colour online.]



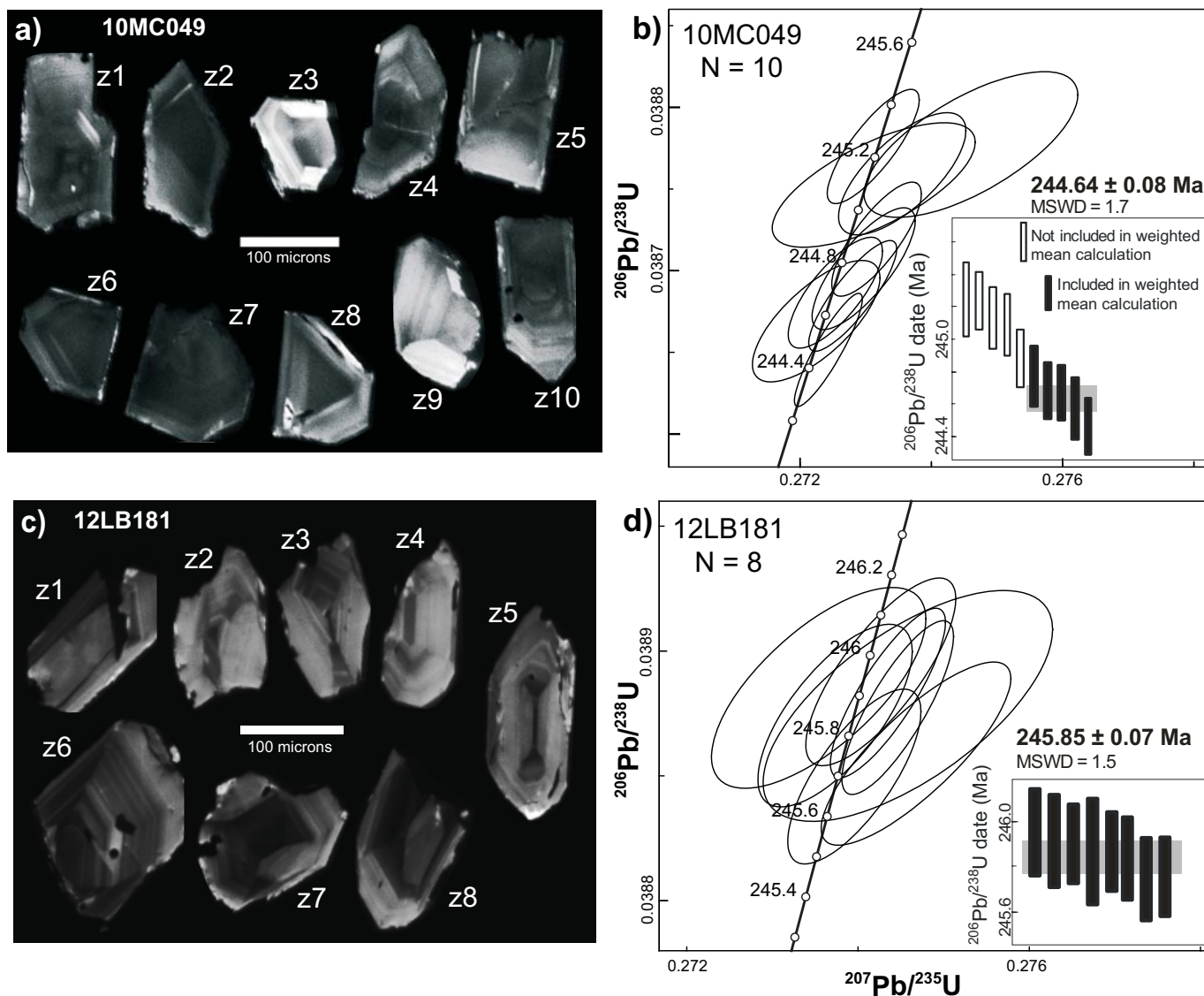
12 Ma (Colpron et al. 2015), with a prominent peak at ca. 198 Ma (Fig. 13), indicating a Sinemurian maximum depositional age for this sample.

$^{40}\text{Ar}/^{39}\text{Ar}$ results

Sample 12LB211 is a pegmatitic biotite–muscovite syenite exposed in the centre of the study area (Fig. 2) that lacked U–Pb-bearing minerals (i.e., zircon, monazite). Both muscovite and biotite yielded moderately complex age spectra with overall dates ranging between ca. 165 and 160 Ma (Fig. 14; Supplementary Table S3¹). The muscovite spectrum shows variable ages for the first 20% of argon released followed by a monotonic age increase from ca. 163.6 to 165.7 Ma for the final eight heating steps. The final two steps of the spectrum define a terminal age of 165.6 ± 0.1 Ma (Fig. 14). The biotite spectrum has an overall hump-shaped pattern defined by initially younger ages that climb to a variable pattern followed by a steep drop for the final heating step. A relatively flat segment of the spectrum yielded an age of 161.7 ± 0.3 Ma for nine steps (Fig. 14).

The muscovite age gradient is likely related to protracted cooling from about 400 to 350 °C (argon closure temperature from Harrison et al. 2009) between ca. 166 and 163 Ma. The biotite age spectrum disturbance can be caused by multiple factors including a protracted cooling history near 300 °C and is also likely impacted by ^{39}Ar recoil (cf., Harrison et al. 1985; Heizler et al. 1988; Lo

Fig. 12. (a) Cathodoluminescence (CL) images of zircon grains chosen for CA-TIMS analysis in sample 10MC049. Labels correspond to zircon analysis provided in Table 3; differences in brightness of CL images indicate differences in U concentration (low = bright; high = dark) and other trace element concentrations. (b) U–Pb concordia plot for sample 10MC049; error ellipses are 2σ . Insets show ranked $^{206}\text{Pb}/^{238}\text{U}$ date plot with weighted mean date represented by grey box behind error bars; errors are 2σ . (c) CL images of zircon grains from sample 12LB181; labels correspond to zircon analysis provided in Table 3. (d) U–Pb concordia plot for sample 12LB181; error ellipses are 2σ . Insets show ranked $^{206}\text{Pb}/^{238}\text{U}$ date plot with weighted mean date represented by grey box behind error bars; errors are 2σ .



and Onstott 1989). Both Heizler et al. (1988) and Lo and Onstott (1989) assigned thermochronological significance to complex biotite spectra and speculated that the integrated age (156.8 ± 0.1 Ma) might record the time of bulk sample cooling near 300°C . Despite somewhat ambiguous interpretations for individual age spectra, the data are broadly consistent with cooling from near 400°C to below 300°C between ca. 165 Ma and 160–155 Ma, and thus supports a Middle Jurassic age for this pluton. These results are inconsistent with previous assignment of this pluton to the mid-Cretaceous Whitehorse plutonic suite (e.g., Gordey and Makepeace 2001); rather, they suggest an affinity with the Middle Jurassic Bryde suite (Colpron et al. 2016).

Discussion

Bedrock mapping at the northern apex of the Cache Creek terrane, near Marsh Lake in southern Yukon, shows that most of the terrane in this region is composed of mafic metavolcanic and

metaplutonic rocks that are structurally imbricated with clastic sedimentary rocks of Stikinia and Whitehorse trough (Fig. 2; Bickerton 2014b). The geochemical signature of the mafic rocks in the Cache Creek terrane suggests that they formed in a magmatic arc derived from a slightly enriched mantle source (Fig. 10), similar to parts of the “oceanic crustal assemblage” in the Nakina area of northern British Columbia (English et al. 2010).

In the Nakina area south of Atlin (Fig. 1), English et al. (2010) documented two prominent geochemical affinities in mafic rocks of the northern Cache Creek terrane. The first is alkaline OIB that crops out in structural panels containing Carboniferous–Permian rocks of the “carbonate assemblage” (Monger 1975). In central British Columbia, rocks of similar character predominate and are interpreted as seamounts that were incorporated in the Cache Creek complex (e.g., Struik et al. 2001; Lapiere et al. 2003). The second geochemical group recognized in the Nakina area form the mid-late Permian to Middle Triassic “oceanic crustal assem-

Fig. 13. (a) Plot of LA-ICPMS $^{206}\text{Pb}/^{238}\text{U}$ dates for zircon grains in sample 12LB220 (plotted with Isoplot 3.0, Ludwig 2003). See inset for example cathodoluminescence images of zircon grains. Bin width in the histograms is the average error on the dates. N, number of grains analyzed. (b) U–Pb concordia plot for sample 12LB220; error ellipses are 2σ .

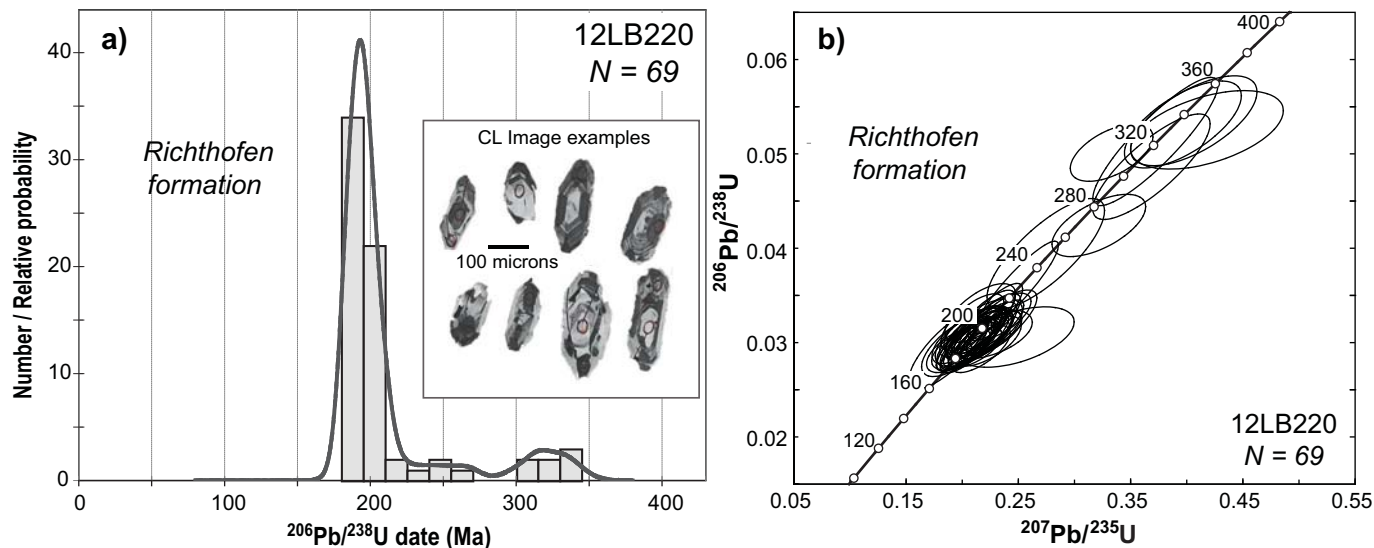
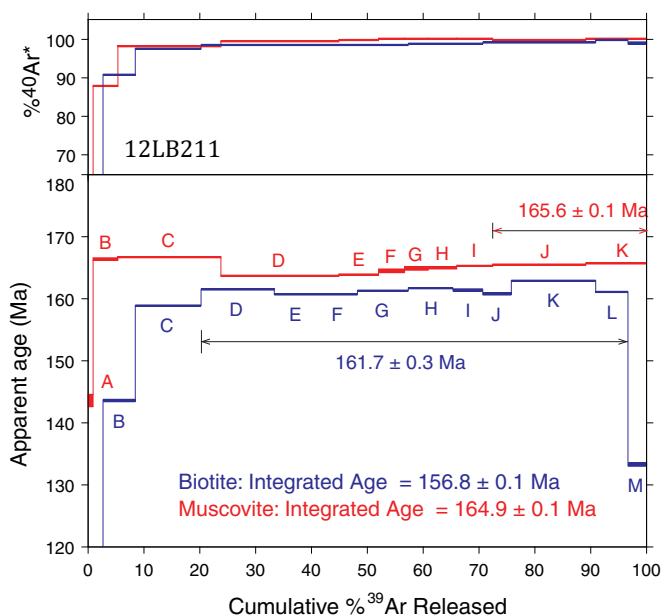


Fig. 14. Age spectra and radiogenic yield plot for micas separated from sample 12LB211, collected from a syenite that intruded rocks of the Whitehorse trough in the field area (Fig. 2). [Colour online.]



blage” (Childe et al. 1998; Devine 2002; Mihalynuk et al. 2003), which includes rocks with island arc tholeiite, calc-alkaline, and back-arc basin affinities (English et al. 2010; McGoldrick et al. 2017; Fig. 10). These subduction-influenced signatures differ from the prominent mantle-derived signature in the Cache Creek terrane of central British Columbia (Lapierre et al. 2003) and suggest that arc crust is a significant component of the northern Cache Creek terrane.

Our mapping near Marsh Lake also identified a new immature clastic unit, the Michie formation (Figs. 2 and 3). It is composed mainly of intra-Cache Creek lithic fragments (Fig. 5) and is in overlying gradational contact with the dominant arc volcanic sequence that characterizes the terrane at its northern apex. Two samples of the Michie formation yielded unimodal, sharply faceted, oscillatory zoned zircon grains with $^{206}\text{Pb}/^{238}\text{U}$ dates of

244.64 ± 0.08 Ma and 245.85 ± 0.07 Ma (Fig. 12). The compositional immaturity of the sandstone (Fig. 5), the sharply faceted and oscillatory zoned zircon grains, and their unimodal U–Pb dates (Figs. 11 and 12) all suggest derivation from a proximal igneous source. Potential sources for ca. 246–245 Ma zircons are limited to the Cache Creek terrane in the northern Cordillera (e.g., Childe and Thompson 1997; R. Friedman in Schiarizza 2012).

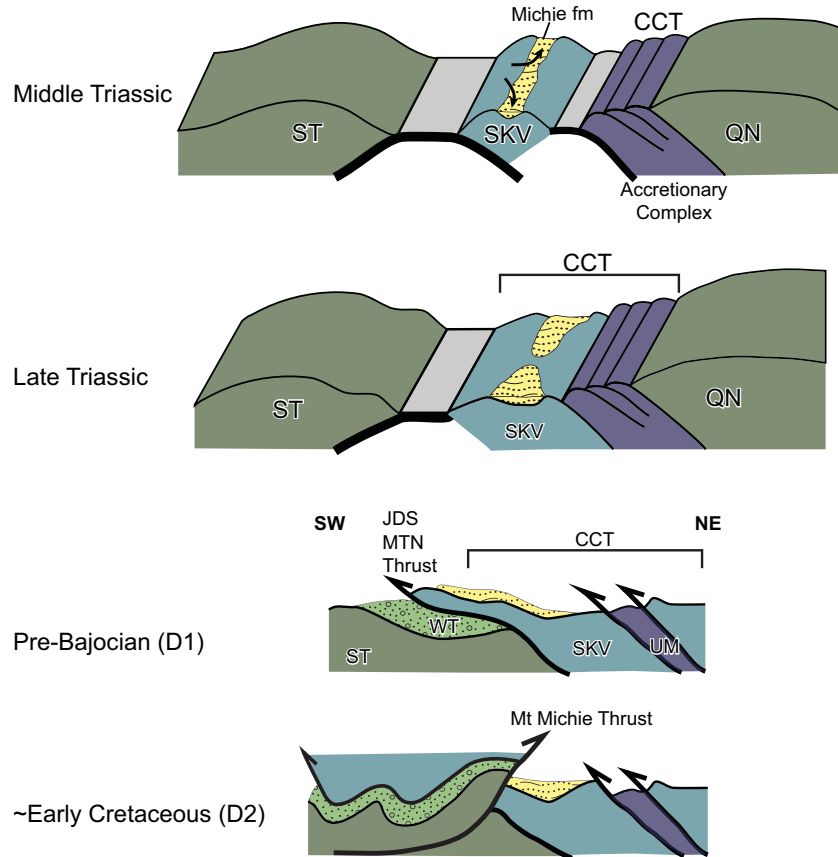
The Kutcho assemblage near Dease Lake in northern British Columbia (Fig. 1) includes bimodal volcanic and volcanoclastic rocks interpreted to have formed in a juvenile oceanic arc setting (Thorstad 1977; Childe and Thompson 1997; Mihalynuk et al. 2003; English et al. 2010; Schiarizza 2012). Eight samples of tonalite, rhyolite, and felsic volcanoclastic rocks from the Kutcho assemblage yielded a range of U–Pb dates from ca. 255 to 242 Ma (Childe and Thompson 1997; Gordey et al. 1998; R. Friedman in Schiarizza 2012), and these rocks represent suitable sources for detritus in the Michie formation to the north.

The Kutcho assemblage is generally considered part of the Cache Creek terrane, although it occupies a lower structural level in the hanging wall of the King Salmon thrust compared with the bulk of the Cache Creek, which lies in the hanging wall of the Nahlin fault (Fig. 1). The association of ultramafic rocks with volcanic and sedimentary rocks of the Kutcho assemblage are key to its affiliation with the Cache Creek terrane (e.g., Gabrielse 1998). The Kutcho assemblage is unconformably overlain by Upper Triassic limestone of the Sinwa Formation and clastic rocks of the Lower Jurassic Inklin Formation (Laberge Group), and this relationship has led others to suggest an affiliation with Stikinia rather than Cache Creek (e.g., English and Johnston 2005). However, recent interpretations show the Laberge Group strata as syn- to post-amalgamation deposits overlapping Stikinia, Cache Creek, Quesnellia, and possibly the Yukon–Tanana terrane as well (Colpron et al. 2015).

Schiarizza (2013) also documented correlatives of the Kutcho assemblage in central and southern British Columbia: the Sitlika and Wineglass assemblages (Fig. 1, inset). They both occupy similar structural positions as the Kutcho assemblage at the base of the Cache Creek terrane and suggest that the Lower to Middle Triassic arc rocks are regionally extensive within the Intermontane terranes.

Arc magmatism in the Cache Creek terrane near Marsh Lake, Yukon, is constrained to be, in part, coeval with Kutcho magma-

Fig. 15. Schematic cross-sectional diagram showing the record of terrane growth and accretion at the northern termination of the Cache Creek terrane in the Canadian Cordillera during the Mesozoic. ST, Stikinia; SKV, Sitlika—Kutcho—Venables arc; CCT, Cache Creek terrane; QN, Quesnellia; WT, Whitehorse trough; JDS MTN, Judas Mountain. [Colour online.]



tism, based on dating of proximally derived detrital zircons from the Michie formation (244.64 ± 0.08 and 245.85 ± 0.07 Ma; Figs. 11 and 12). A similar U–Pb zircon date of 245.4 ± 0.8 Ma is reported by Gordey et al. (1998) from a gabbro body associated with peridotite east of the present study area (Fig. 1). Studies of ultramafic rocks near Atlin, British Columbia (Fig. 1), concluded that they originated in a supra-subduction zone setting, rather than at a MORB seafloor spreading centre (Ash 1994; Mihalynuk et al. 2003; Zagorevski et al. 2015; McGoldrick et al. 2017). Collectively, these findings suggest that mafic and ultramafic igneous rocks in the northern Cache Creek terrane represent fragments of intra-oceanic arc lithosphere. These rocks are coeval with and formed in a similar setting as those of the Kutcho assemblages and correlatives elsewhere in British Columbia; they may have developed as contiguous intra-oceanic arcs in Early to Middle Triassic, or as isolated fragments juxtaposed during Jurassic terrane accretion (Golding 2018).

Accretion of Kutcho (and correlatives) intra-oceanic arc fragment(s) at the end of the Triassic is inferred to have led to slab tear and demise of the Triassic subduction beneath Stikinia and Quesnellia (Logan and Mihalynuk 2014). Regional stratigraphic, structural, metamorphic, and geochronological evidence indicate onset of orogenesis (crustal thickening), uplift, and exhumation in latest Triassic to Early Jurassic in the northern Cordillera (Colpron et al. 2015, and references therein). This is reflected in the detrital zircon population from our sample of Richthofen formation (12LB220; Fig. 13) that shows a shift in source regions with a prominent peak at ca. 198 Ma and a minor peak at 340–300 Ma. The few zircons in the 260–240 Ma range (Fig. 13) likely reflect minor contribution from a Kutcho-like source or recycling of the Michie formation.

Imbrication of the Cache Creek terrane with adjacent rocks of Stikinia and Whitehorse trough is interpreted to result from two distinct episodes of contractional deformation based on our structural observations from the Marsh Lake area (Figs. 2 and 6). A first phase of southwest-vergent thrusting (D_1) emplaced Triassic volcanic rocks of the Cache Creek terrane over Jurassic clastic rocks of the Whitehorse trough along the Judas Mountain thrust (Fig. 15). The Judas Mountain thrust is likely an equivalent to the Nahlin fault in northern British Columbia (Hart and Radloff 1990; Gabrielse 1991, 1998; Mihalynuk 1999; Mihalynuk et al. 2004; Evenchick et al. 2005), offset along the Crag Lake fault in southern Yukon (Fig. 1). In northern British Columbia, timing of southwest-vergent thrust imbrication is constrained to postdate Toarcian sedimentation but predate emplacement of ca. 172 Ma plutons, such as the Fourth of July batholith near Atlin (Mihalynuk et al. 2004; Fig. 1). The Middle Jurassic $^{40}\text{Ar}/^{39}\text{Ar}$ mica cooling ages from a syenite pluton intruding Stikinia and Whitehorse trough near Marsh Lake (Fig. 14) suggest that magmas related to the Fourth of July batholith also intruded the footwall of the Cache Creek complex.

Early to Middle Jurassic imbrication of Stikinia, Cache Creek, and Quesnellia has been explained by oroclinal enclosure of the Cache Creek terrane and inferred southward propagation of deformation (Mihalynuk et al. 1994, 2004; Colpron et al. 2015). The Middle Jurassic exhumation of the Cache Creek terrane is expressed by influx of chert-rich detritus in Bajocian and younger strata of Bowser Lake Group in British Columbia (e.g., Ricketts et al. 1992; Evenchick et al. 2010), and Bathonian–Callovian conglomerate of the Tantalus Formation in Yukon (Long 2005; Colpron et al. 2015).

The second phase of deformation (D_2) involved northeast-vergent thrust imbrication and related folding (Figs. 2, 6, and 15).

The main structure associated with the D₂ phase in the Marsh Lake area is the south–southeast-striking, northeast-verging Mount Michie thrust (Figs. 2 and 6). The Mount Michie thrust juxtaposes Upper Triassic rocks of the Lewes River Group (Stikinia; which are interpreted to occupy the footwall of the D₁ Judas Mountain thrust) to the southwest, against Middle Triassic rocks of the Cache Creek terrane to the northeast (hanging wall of D₁ Judas Mountain thrust). The D₂ deformation resulted in tight folding of the Judas Mountain thrust near Marsh Lake (Figs. 2, 6, and 15).

The timing of D₂ deformation is poorly constrained in the Marsh Lake area. The Mount Michie thrust and related folds appear to be intruded by plutons assigned to the mid-Cretaceous (ca. 112–105 Ma) Whitehorse plutonic suite north of Marsh Lake (Fig. 2). A K–Ar date of ca. 104 Ma from a small pluton along the Alaska Highway at Marsh Lake (Hart 1995) supports the interpretation that the Whitehorse plutonic suite extends to this area. However, our Middle Jurassic ⁴⁰Ar/³⁹Ar dates from a pluton east of Marsh Lake cast doubts on the age of undated plutons near the north end of the study area (Fig. 2).

Based on regional considerations, northeast-verging structures in southern Yukon may be coeval with the Late Jurassic to Early Cretaceous (Oxfordian to Albian) development of the Skeena fold and thrust belt in central British Columbia (Evenchick 1991; Evenchick et al. 2007). Alternatively, they could be related to mid-Cretaceous (ca. 115–95 Ma) dextral transpression associated with development of regional, dextral strike-slip faults such as the Teslin–Thibert fault system in southern Yukon and northern British Columbia (Fig. 1; Gabrielse et al. 2006; White et al. 2012; Nelson et al. 2013; Calvert et al. 2017).

Conclusion

The northern termination of the Cache Creek terrane in southern Yukon is mainly composed of mafic metavolcanic and metavolcaniclastic rocks, and mafic to ultramafic ophiolitic complexes that represent remnant of an intra-oceanic arc succession. Immature clastic rocks at the top of the metavolcanics succession, the Michie formation, yielded first-cycle zircons with Middle Triassic dates of 244.64 ± 0.08 Ma and 245.85 ± 0.07 Ma, suggesting correlation with other intra-oceanic arc rocks of the Kutcho, Sitlika, and Wineglass assemblages to the south. Rocks of the Cache Creek terrane in southern Yukon are imbricated with sedimentary rocks of Stikinia and Whitehorse trough near Marsh Lake, Yukon. The first phase of southwest-verging folding and thrusting correspond with terrane accretion structures, documented in northern British Columbia, and are intruded by Middle Jurassic plutons. A second phase of thrusting resulted in reshuffling of the original terrane stacking, and likely relates to regional Early Cretaceous dextral transpression.

Acknowledgements

Funding for this project was provided by the Yukon Geological Survey (YGS), Northern Scientific Training Program (NSTP), and by Natural Science and Engineering Research Council (NSERC) grants to H.D. Gibson and M. Colpron. Thanks to Cam Dorsey and Jaap Verbaas for assistance in the field, and to staff at the YGS and Simon Fraser University for support during this study. We thank Steve Piercey (Memorial University) for providing unpublished geochemical data from the Marsh Lake area. Joanne Nelson and Don Murphy provided constructive comments on an earlier version of this manuscript. Journal reviews by Bram van Stratten and two anonymous reviewers helped improve the final manuscript. This is Yukon Geological Survey contribution No. 041.

References

Armstrong, R.L. 1988. Mesozoic and early Cenozoic magmatic evolution of the Canadian Cordillera. *Geological Society of America Special Papers*, **218**: 55–

- Ash, C.H. 1994. Origin and tectonic setting of ophiolitic ultramafic and related rocks in the Atlin area, British Columbia (NTS 104N). B.C. Ministry of Energy, Mines and Petroleum Resources, Bulletin 94, 48 p.
- Barrett, T.J., and MacLean, W.H. 1999. Volcanic sequences, litho-geochemistry, and hydrothermal alteration in some bimodal volcanic-associated massive sulfide systems. In *Volcanic-associated massive sulfide deposits: processes and examples in modern and ancient environments*. Edited by C.T. Barrie and M.D. Hannington. Society of Economic Geologists, Reviews in Economic Geology, **8**: 101–131. doi:10.5382/Rev.08.05.
- B.C. Geological Survey. 2015. British Columbia Digital Geology. <https://www2.gov.bc.ca/gov/content/industry/mineral-exploration-mining/british-columbia-geological-survey/geology/bcdigitalgeology> [accessed December 23, 2015].
- Belasky, P., Stevens, C.H., and Hanger, R.A. 2002. Early Permian location of western North American terranes based on brachiopod, fusulinid, and coral biogeography. *Palaeogeography, Palaeoclimatology, Palaeoecology*, **179**: 245–266. doi:10.1016/S0031-0182(01)00437-0.
- Bickerton, L. 2014a. The northern Cache Creek terrane: record of Middle Triassic arc activity and Jurassic-Cretaceous terrane imbrication. Unpublished M.Sc. thesis, Simon Fraser University, Burnaby, British Columbia. 105 p.
- Bickerton, L. 2014b. Geological map of Michie Creek (NTS 105D/9) and parts of Tagish (NTS 105D/8) areas. Yukon Geological Survey, 2014-11, 1:50,000.
- Bordet, E. 2018. Bedrock geology of the Teslin Mountain and east Lake Laberge areas, south-central Yukon. In *Yukon exploration and geology 2017*. Edited by K.E. MacFarlane. Yukon Geological Survey, pp. 1–24.
- Calvert, A.J., Hayward, N., Vayavur, R., and Colpron, M. 2017. Seismic and gravity constraints on the crustal architecture of the Intermontane terranes, central Yukon. *Canadian Journal of Earth Sciences*, **54**(7): 798–811. doi:10.1139/cjes-2016-0189.
- Canil, D., Mihalynuk, M., and Charnell, C. 2006. Sedimentary record for exhumation of ultrahigh pressure (UHP) rocks in the northern Cordillera, British Columbia, Canada. *Geological Society of America Bulletin*, **118**: 1171–1184. doi:10.1130/B25921.1.
- Childe, F.C., and Thompson, J.F.H. 1997. Geological setting, U-Pb geochronology, and radiogenic isotopic characteristics of the Permo-Triassic Kutcho Assemblage, north-central British Columbia. *Canadian Journal of Earth Sciences*, **34**(10): 1310–1324. doi:10.1139/e17-104.
- Childe, F.C., Thompson, J.F.H., Mortensen, J.K., Friedman, R.M., Schiarizza, P., Bellefontaine, K., and Marr, J.M. 1998. Primitive Permo-Triassic volcanism in the Canadian Cordillera: Tectonic and metallogenetic implications. *Economic Geology*, **93**: 224–231. doi:10.2113/gsecongeo.93.2.224.
- Colpron, M. 2011. Geological compilation of Whitehorse trough - Whitehorse (105D), Lake Laberge (105E), and part of Carmacks (115I), Glenlyon (105L), Aishihik Lake (115H), Quiet Lake (105F) and Teslin (105C). Yukon Geological Survey, Geoscience Map 2011-1, 1:250 000.
- Colpron, M., and Nelson, J.L. 2011. A digital atlas of terranes for the northern Cordillera: Yukon Geological Survey, www.geology.gov.yk.ca/bedrock_terrane.html, accessed September 2013; also British Columbia Ministry of Energy and Mines, BCGS GeoFile 2011-11.
- Colpron, M., Nelson, J.L., and Murphy, D.C. 2006. A tectonostratigraphic framework for the pericratonic terranes of the northern Cordillera. In *Paleozoic Evolution and Metallogeny of Pericratonic Terranes at the Ancient Pacific Margin of North America, Canadian and Alaskan Cordillera*. Edited by M. Colpron and J.L. Nelson. Geological Association of Canada, Special Paper, **45**, pp. 1–23.
- Colpron, M., Crowley, J.L., Gehrels, G.E., Long, D.G.F., Murphy, D.C., Beranek, L.P., and Bickerton, L. 2015. Birth of the northern Cordilleran orogen, as recorded by detrital zircons in Jurassic synorogenic strata and regional exhumation in Yukon. *Lithosphere*, **7**: 541–562. doi:10.1130/L1451.1.
- Colpron, M., Israel, S., Murphy, D.C., Pigage, L.C., and Moynihan, D. 2016. Yukon Bedrock Geology Map 2016. Yukon Geological Survey, Open File 2016-1, 1:1,000,000 scale.
- Coney, P.J., Jones, D.L., and Monger, J.W.H. 1980. Cordilleran suspect terranes. *Nature*, **288**: 329–333. doi:10.1038/288329a0.
- Cordey, F., Gordey, S.P., and Orchard, M.J. 1991. New biostratigraphic data from the northern Cache Creek terrane, Teslin map area, southern Yukon. In *Current Research part E, Geological Survey of Canada*, pp. 67–76.
- Crowley, J.L., Schoene, B., and Bowring, S.A. 2007. U-Pb dating of zircon in the Bishop Tuff at the millennial scale. *Geology*, **35**: 1123–1126. doi:10.1130/G24017A.1.
- Devine, F.A.M. 2002. U–Pb geochronology, geochemistry, and tectonic implications of oceanic rocks in the northern Cache Creek Terrane, Nakina area, northwestern British Columbia. B.Sc. thesis, The University of British Columbia, Vancouver, B.C.
- Dickinson, W.R. 1970. Interpreting detrital modes of greywacke and arkose. *Journal of Sedimentary Research*, **40**: 695–707. doi:10.1306/74D72018-2B21-11D7-8648000102C1865D.
- Dickinson, W.R., Beard, L.S., Brakenridge, G.R., Erjavec, J.L., Ferguson, R.C., Inman, K.F., et al. 1983. Provenance of North American Phanerozoic sandstones in relation to tectonic setting. *Geological Society of America Bulletin*, **94**: 222–235. doi:10.1130/0016-7606(1983)94<222:PONAPS>2.0.CO;2.
- Dostal, J., Gale, V., and Church, B.N. 1999. Upper Triassic Takla Group volcanic rocks, Stikine Terrane, north-central British Columbia: geochemistry, petro-

- genesis, and tectonic implications. *Canadian Journal of Earth Sciences*, **36**(9): 1483–1494. doi:10.1139/e99-048.
- Dostal, J., Keppie, J.D., and Ferri, F. 2009. Extrusion of high-pressure Cache Creek rocks into the Triassic Stikinia-Quesnellia arc of the Canadian Cordillera: implications for terrane analysis of ancient orogens and palaeogeography. *Geological Society, London, Special Publications*, **327**: 71–87. doi:10.1144/SP327.5.
- English, J. 2004. Convergent margin tectonics in the North American Cordillera: implications for continental growth orogeny. Unpublished Ph.D. thesis, University of Victoria, Victoria, British Columbia. 204 p.
- English, J.M., and Johnston, S.T. 2005. Collisional orogenesis in the northern Canadian Cordillera: Implications for Cordilleran crustal structure, ophiolite emplacement, continental growth, and the terrane hypothesis. *Earth and Planetary Science Letters*, **232**: 333–344. doi:10.1016/j.epsl.2005.01.025.
- English, J.M., Mihalynuk, M.G., and Johnston, S.T. 2010. Geochemistry of the northern Cache Creek terrane and implications for accretionary processes in the Canadian Cordillera. *Canadian Journal of Earth Sciences*, **47**(1): 13–34. doi:10.1139/E09-066.
- Evenchick, C.A. 1991. Structural relationships of the Skeena Fold Belt west of the Bowser Basin, Northwest British Columbia. *Canadian Journal of Earth Sciences*, **28**(6): 973–983. doi:10.1139/e91-088.
- Evenchick, C.A., Gabrielse, H., Cook, F.A., Clowes, R.M., Snyder, D.B., van der Velden, A.J., et al. 2001. Highlights of SNORCLE Line 2A—The Cassiar-Stewart Highway (Highway 37, 37A). In *Slave–Northern Cordillera Lithospheric Evolution (SNORCLE) Transect and Cordilleran Tectonics Workshop Meeting*, Lithoprobe Report No. 79, Pacific Geoscience Centre, Sydney, Edited by F. Cook and P. Erdmer, pp. 56–58.
- Evenchick, C.A., Gabrielse, H., and Snyder, D. 2005. Crustal structure and lithology of the northern Canadian Cordillera: alternative interpretations of SNORCLE seismic reflection lines 2a and 2b. *Canadian Journal of Earth Sciences*, **42**(6): 1149–1161. doi:10.1139/e05-009.
- Evenchick, C.A., McMechan, M.E., McNicoll, V.J., and Carr, S.D. 2007. A synthesis of the Jurassic-Cretaceous tectonic evolution of the central and southeastern Canadian Cordillera: Exploring links across the orogen. *Geological Society of America, Special Paper*, **433**: 117–145. doi:10.1130/2007.2433(06).
- Evenchick, C.A., Poulton, T.P., and McNicoll, V.J. 2010. Nature and significance of the diachronous contact between the Hazelton and Bowser Lake groups (Jurassic), north-central British Columbia. *Bulletin of Canadian Petroleum Geology*, **58**: 235–267. doi:10.2113/gscpgbull.58.3.235.
- Gabrielse, H. 1991. Late Paleozoic and Mesozoic terrane interactions in north-central British Columbia. *Canadian Journal of Earth Sciences*, **28**(6): 947–957. doi:10.1139/e91-086.
- Gabrielse, H. 1998. Geology of Dease Lake (104J) and Cry Lake (104I) map areas, north-central British Columbia. *Geological Survey of Canada, Bulletin*, **504**. doi:10.4095/210074.
- Gabrielse, H., Murphy, D.C., and Mortensen, J.K. 2006. Cretaceous and Cenozoic dextral orogen-parallel displacements, magmatism and paleogeography, north-central Canadian Cordillera. In *Paleogeography of the North American Cordillera: Evidence for and against large-scale displacements*. Edited by J.W. Haggart, J.W.H. Monger, and R.J. Enkin. *Geological Association of Canada Special Paper*, **46**: 255–276.
- Gibson, S.A., Kirkpatrick, R.J., Emmerman, R., Schmincke, P.-H., Pritchard, G., Okay, P.J., et al. 1982. The trace element composition of the lavas and dykes from a 3 km vertical section through a lava pile of Eastern Iceland. *Journal of Geophysical Research*, **87**: 6532–6546. doi:10.1029/JB087iB08p06532.
- Gill, J.B. 1981. *Orogenic andesites and plate tectonics*. Springer-Verlag, Berlin. 390 p.
- Golding, M.L. 2018. Heterogeneity of conodont faunas in the Cache Creek Terrane, Canada: significance for tectonic reconstructions of the North American Cordillera. *Palaeogeography, Palaeoclimatology, Palaeoecology*, **506**: 208–216. doi:10.1016/j.palaeo.2018.06.038.
- Gordey, S.P., and Makepeace, A.J. 2001. Bedrock geology, Yukon Territory. *Geological Survey of Canada, Open File 3754*, 1:1 000 000. Also: Yukon Geological Survey, Open File 2001-1.
- Gordey, S.P., and Stevens, R.A. 1994. Geology, Teslin, Yukon Territory. *Geological Survey of Canada, Open File 2886*, 1:250 000 scale.
- Gordey, S.P., McNicoll, V.J., and Mortenson, J.K. 1998. New U-Pb ages from the Teslin area, southern Yukon, and their bearing on terrane evolution in the northern Cordillera. In *Radiogenic age and isotopic studies*. Report 11, Geological Survey of Canada, Current Research no. 1998-F, pp. 129–148.
- Harrison, T.M., Duncan, I., and McDougall, I. 1985. Diffusion of ⁴⁰Ar in biotite: Temperature, pressure and compositional effects. *Geochimica et Cosmochimica Acta*, **49**: 2461–2468. doi:10.1016/0016-7037(85)90246-7.
- Harrison, T.M., Celerier, J., Aikman, A., Hermann, J., and Heizler, M.T. 2009. Diffusion of ⁴⁰Ar in muscovite. *Geochimica et Cosmochimica Acta*, **73**: 1039–1051. doi:10.1016/j.gca.2008.09.038.
- Hart, C.J.R. 1995. Magmatic and tectonic evolution of the Intermontane Superterrane and Coast Plutonic Complex in southern Yukon Territory. Unpublished M.Sc. thesis, The University of British Columbia, 198 p.
- Hart, C.J.R. 1997. A transect across Northern Strikinia: Geology of the Northern Whitehorse Map Area, Southern Yukon Territory (105D/13-16), Canada. Dept. of Indian Affairs Northern Development. *Exploration Geological Services Division, Yukon Region*.
- Hart, C.J.R., and Radloff, J.K. 1990. Geology of the Whitehorse, Alligator Lake, Fenwick Creek, Carcross and part of Robinson map areas (105D/11.6,3,2&7), Yukon Territory. *Exploration and Geological Services Division, Yukon Region, Indian and Northern Affairs Canada, Open File 1990-4*, 113 p.
- Heizler, M.T., Lux, D.R., and Decker, E.R. 1988. The age and cooling history of the Chain of Ponds and Big Island Pond plutons and the Spider Lake Granite, west-central Maine and Quebec. *American Journal of Science*, **288**: 925–952. doi:10.2475/ajs.288.9.925.
- Helwig, J. 1974. Eugeosynclinal basement and a collage concept of orogenic belts. In *Modern and ancient geosynclinal sedimentation*. Edited by R.H. Dott, Jr. and R.H. Shaver. *Society of Economic Paleontologists and Mineralogists, Special Publication 19*, pp. 359–380.
- Ingersoll, R.V. 1978. Petrofacies and petrologic evolution of the Late Cretaceous Fore-arc Basin, Northern and Central California. *The Journal of Geology*, **86**: 335–352. doi:10.1086/649695.
- Ingersoll, R.V., Fullard, T.F., Ford, R.L., Grimm, J.P., Pickle, J.D., and Sares, S.W. 1984. The effect of grain size on detrital modes; a test of the Gazzi-Dickinson point-counting method. *Journal of Sedimentary Research*, **54**: 103–116. doi:10.1306/212F83B9-2B24-11D7-8648000102C1865D.
- Jackson, J.L. 1992. Tectonic analysis of the Nisling, northern Stikine and northern Cache Creek Terranes, Yukon and British Columbia. Unpublished Ph.D. thesis, The University of Arizona, Tucson, 200 p.
- Jackson, J.L., Gehrels, G.E., Patchett, P.J., and Mihalynuk, M.G. 1991. Stratigraphic and isotopic link between the northern Stikine terrane and an ancient continental margin assemblage, Canadian Cordillera. *Geology*, **19**: 1177–1180. doi:10.1130/0091-7613(1991)019<1177:SAILBT>2.3.CO;2.
- Jaffey, A.H., Flynn, K.F., Glendenin, L.E., Bentley, W.C., and Essling, A.M. 1971. Precision measurement of half-lives and specific activities of ²³⁵U and ²³⁸U. *Physical Review C*, **4**: 1889–1906. doi:10.1103/PhysRevC.4.1889.
- Johnston, S.T., and Borel, G.D. 2007. The odyssey of the Cache Creek terrane, Canadian Cordillera: Implications for accretionary orogens, tectonic setting of Panthalassa, the Pacific superwell, and break-up of Pangea. *Earth and Planetary Science Letters*, **253**: 415–428. doi:10.1016/j.epsl.2006.11.002.
- Kuiper, K.F., Deino, A., Hilgen, F.J., Krijgsman, W., Renne, P.R., and Wijbrans, J.R. 2008. Synchronizing the rock clocks of Earth history. *Science*, **320**: 500–504. doi:10.1126/science.1154339. PMID:18436783.
- Lapierre, H., Bosch, D., Tardy, M., and Struik, L.C. 2003. Late Paleozoic and Triassic plume-derived magmas in the Canadian Cordillera played a key role in continental crust growth. *Chemical Geology*, **201**: 55–89. doi:10.1016/S0009-2541(03)00224-9.
- Lees, E.J. 1934. Geology of the Laberge area, Yukon. *Transactions of the Royal Canadian Institute*, **20**: 1–48.
- Lo, C.-H., and Onstott, T.C. 1989. ³⁹Ar recoil artifacts in chloritized biotite. *Geochimica et Cosmochimica Acta*, **53**: 2967–2711. doi:10.1016/0016-7037(89)90141-5.
- Logan, J.M., and Mihalynuk, M.G. 2014. Tectonic controls on early Mesozoic paired alkaline porphyry deposit belts (Cu-Au ± Ag-Pt-Pd-Mo) within the Canadian Cordillera. *Economic Geology and the Bulletin of the Society of Economic Geologists*, **109**: 827–858. doi:10.2113/econgeo.109.4.827.
- Long, D.G.F. 2005. Sedimentology and hydrocarbon potential of fluvial strata in the Tantalus and Aksala formations, northern Whitehorse Trough, Yukon. In *Yukon Exploration and Geology 2005*, p. 9.
- Long, D.G.F. 2015. Provenance and depositional framework of braided and meandering gravel-bed river deposits and associated coal deposits in active intermontane piggyback basins: The Upper Jurassic to Lower Cretaceous Tantalus Formation, Yukon. *Yukon Geological Survey, Open File 2015-23*, 80 p.
- Love, D.A., Clark, A.H., Hodgson, C.J., Mortensen, J.K., Archibald, D.A., and Farrar, E. 1998. The timing of adularia-sericite-type mineralization and alunite-kaolinite-type alteration, Mount Skukum epithermal gold deposit, Yukon Territory, Canada, ⁴⁰Ar-³⁹Ar and U-Pb geochronology. *Economic Geology*, **93**: 437–462. doi:10.2113/gsecongeo.93.4.437.
- Lowey, G.W. 2004. Sedimentology, stratigraphy and source rock potential of the Richthofen formation (Jurassic), northern Whitehorse Trough. In *Yukon Exploration and Geology 2004*. Edited by D.S. Edmond, L.L. Lewis, and G.D. Bradshaw. *Yukon Geological Survey*, pp. 177–191.
- Lowey, G.W., Long, D.G.F., Fowler, M.G., Sweet, A.R., and Orchard, M.J. 2009. Petroleum source rock potential of Whitehorse trough: a frontier basin in south-central Yukon. *Bulletin of Canadian Petroleum Geology*, **57**: 350–386. doi:10.2113/gscpgbull.57.3.350.
- Ludwig, K.R. 2003. *User's manual for Isoplot 3.00*. Berkeley Geochronology Center, Berkeley, Calif., 70 p.
- Mattinson, J.M. 2005. Zircon U-Pb chemical abrasion (“CA-TIMS”) method: combined annealing and multi-step partial dissolution analysis for improved precision and accuracy of zircon ages. *Chemical Geology*, **220**: 47–66. doi:10.1016/j.chemgeo.2005.03.011.
- McClelland, W.C. 1992. Permian and older rocks of the southwestern Iskut River map area, northwestern British Columbia: Current research, part A. *Geological Survey of Canada, Paper*, pp. 303–307.
- McGoldrick, S., Zagorevski, A., and Canil, D. 2017. Geochemistry of volcanic and plutonic rocks from the Nahlin ophiolite with implications for a Permian-Triassic arc in the Cache Creek terrane, northwestern British Columbia. *Canadian Journal of Earth Sciences*, **54**(12): 1214–1227. doi:10.1139/cjes-2017-0069.

- Mihalynuk, M.G. 1999. Geology and mineral resources of the Tagish Lake area (NTS 104M/8, 9, 10E, 15 and 104N/12W), Northwestern British Columbia. BCGS Bulletin 105, 293 p.
- Mihalynuk, M.G., Nelson, J., and Diakow, L.J. 1994. Cache Creek Terrane entrapment: oroclinal paradox within the Canadian Cordillera. *Tectonics*, **13**: 575–595. doi:10.1029/93TC03492.
- Mihalynuk, M.G., Johnston, S.T., English, J.M., Cordey, F., Villeneuve, M.E., Rui, L., and Orchard, M.J. 2003. Atlin TGI, Part II: Regional geology and mineralization of the Nakina area (NTS 104N/2W and 3). In *Geological fieldwork 2002*; British Columbia Ministry of Energy and Mines, pp. 9–37.
- Mihalynuk, M.G., Erdmer, P., Ghent, E.D., Cordey, F., Archibald, D.A., Friedman, R.M., and Johannson, G.G. 2004. Coherent French Range blueschist: Subduction to exhumation in <2.5 m.y.? *Geological Society of America Bulletin*, **116**: 910–922. doi:10.1130/B25393.1.
- Miller, M.M. 1987. Dispersed remnants of a northeast Pacific fringing arc: Upper Paleozoic terranes of Permian McCloud faunal affinity, Western U.S. *Tectonics*, **6**: 807–830. doi:10.1029/TC006i006p0807.
- Miskovic, A., and Francis, D. 2004. The Early Tertiary Sifton Range volcanic complex, southwestern Yukon. In *Yukon exploration and geology 2003*. Edited by D.S. Edmond and L.L. Lewis. Yukon Geological Survey, pp. 143–155.
- Monger, J.W.H. 1975. Upper Paleozoic rocks of the Atlin Terrane. Geological Survey of Canada, Paper 74-47, 63 p.
- Monger, J.W.H., and Nokleberg, W.J. 1996. Evolution of the northern North American Cordillera: generation, fragmentation, displacement and accretion of successive North American plate margin arcs. In *Geology and ore deposits of the American Cordillera*. Edited by A.R. Coynor and P.L. Fahey. Geological Society of Nevada Symposium Proceedings, Reno–Sparks, Nev., April 1995, pp. 1133–1152.
- Monger, J.W.H., and Ross, C.A. 1971. Distribution of fusulinaceans in the western Canadian Cordillera. *Canadian Journal of Earth Sciences*, **8**(2): 259–278. doi:10.1139/e71-026.
- Monger, J.W.H., Price, R.A., and Tempelman-Kluit, D.J. 1982. Tectonic accretion and the origin of the two major metamorphic and plutonic belts in the Canadian Cordillera. *Geology* (Boulder), **10**: 70–75. doi:10.1130/0091-7613(1982)10<70:TAATOO>2.0.CO;2.
- Monger, J.W.H., Wheeler, J.O., Tipper, H.W., Gabrielse, H., Harms, T., Struik, L.C., et al. 1991. Cordilleran terranes. In *Geology of the Cordilleran orogen in Canada*. Edited by H. Gabrielse and C.J. Yorath. Geological Survey of Canada, *Geology of Canada*, **4**: 281–327.
- Mortimer, N. 1987. The Nicola Group: Late Triassic and Early Jurassic subduction-related volcanism in British Columbia. *Canadian Journal of Earth Sciences*, **24**(12): 2521–2536. doi:10.1139/e87-236.
- Nelson, J.L., and Friedman, R. 2004. Superimposed Quesnel (late Paleozoic–Jurassic) and Yukon-Tanana (Devonian–Mississippian) arc assemblages, Cassiar Mountains, northern British Columbia; field, U-Pb, and igneous petrochemical evidence. *Canadian Journal of Earth Sciences*, **41**(10): 1201–1235. doi:10.1139/e04-028.
- Nelson, J.L., Colpron, M., Piercey, S.J., Dusel-Bacon, C., Murphy, D.C., and Roots, C.F. 2006. Paleozoic tectonic and metallogenic evolution of the pericratonic terranes in Yukon, northern British Columbia and eastern Alaska. In *Paleozoic evolution and metallogeny of pericratonic terranes at the Ancient Pacific Margin of North America*, Canadian and Alaskan Cordillera. Edited by M. Colpron and J.L. Nelson. Geological Association of Canada, Special Paper 45, pp. 323–360.
- Nelson, J.L., Colpron, M., and Israel, S. 2013. The Cordillera of British Columbia, Yukon, and Alaska: Tectonics and metallogeny. In *Tectonics, metallogeny and discovery: the North American Cordillera and similar accretionary settings*. Edited by M. Colpron, T. Bissig, B.G. Rusk, and J.F.H. Thompson. Society of Economic Geologists, Inc., Special Publication 17, pp. 53–103.
- Nokleberg, W.J., Parfenov, L.M., Monger, J.W.H., Norton, I.O., Khanchuk, A.I., Stone, D.B., et al. 2000. Phanerozoic tectonic evolution of the circum-North Pacific. U.S. Geological Survey Professional Paper 1626, 122 p.
- Orchard, M.J., Cordey, F., Rui, L., Bamber, E.W., Mamet, B., Struik, L.C., et al. 2001. Biostratigraphic and biogeographic constraints on the Carboniferous to Jurassic Cache Creek Terrane in central British Columbia. *Canadian Journal of Earth Sciences*, **38**(4): 551–578. doi:10.1139/e00-120.
- Pearce, J.A. 1983. Role of the sub-continental lithosphere in magma genesis at active continental margins. In *Continental basalts and mantle xenoliths*. Edited by C.J. Hawkesworth and M.J. Norry. Nantwich, Cheshire, pp. 230–249.
- Pearce, J., and Peate, D. 1995. Tectonic implications of the composition of volcanic arc magmas. *Annual Review of Earth and Planetary Sciences*, **23**: 251–286. doi:10.1146/annurev.ea.23.050195.001343.
- Piercey, S.J., Murphy, D.C., Mortensen, J.K., and Creaser, R.A. 2004. Mid-Paleozoic initiation of the northern Cordilleran marginal back-arc basin: Geological, geochemical and neodymium isotopic evidence from the oldest mafic magmatic rocks in Yukon-Tanana terrane, Finlayson Lake district, southeast Yukon, Canada. *Geological Society of America Bulletin*, **116**: 1087–1106. doi:10.1130/B25162.1.
- Ricketts, B.D., Evenchick, C.A., Anderson, R.G., and Murphy, D.C. 1992. Bowser basin, northern British Columbia: Constraints on the timing of initial subsidence and Stikinia-North America terrane interactions. *Geology*, **20**: 1119–1122. doi:10.1130/0091-7613(1992)020<1119:BBNBCC>2.3.CO;2.
- Ruks, T.W., Piercey, S.J., Ryan, J.J., Villeneuve, M.E., and Creaser, R.A. 2006. Mid- to Late Paleozoic K-Feldspar Auger Granitoids of the Yukon-Tanana Terrane, Yukon, Canada: Implications for Crustal Growth and Tectonic Evolution of the Northern Cordillera. *Geological Society of America Bulletin*, **118**: 1212–1231. doi:10.1130/B25854.1.
- Schiarrizza, P. 2011. Geology of the Kutcho Assemblage between Kutcho Creek and the Tucho River, Northern British Columbia (NTS 104J/01). Paper - Ministry of Energy, Mines and Petroleum Resources, pp. 99–118.
- Schiarrizza, P. 2012. Bedrock geology of the upper Kutcho Creek area, parts of NTS 104-J/01, 02. Open-File Report - Geological Survey of Canada, 2012-08: scale 1:40 000.
- Schiarrizza, P. 2013. The Wineglass assemblage, lower Chilcotin River, south-central British Columbia: Late Permian volcanic and plutonic rocks that correlate with the Kutcho assemblage of northern British Columbia. In *Geological Fieldwork 2012*, British Columbia Ministry of Energy, Mines and Natural Gas, British Columbia Geological Survey Paper 2013-1, pp. 53–70.
- Schmitz, M.D., and Schoene, B. 2007. Derivation of isotope ratios, errors and error correlations for U-Pb geochronology using ²⁰⁵Pb-²³⁵U-(²³³U)-spiked isotope dilution thermal ionization mass spectrometric data. *Geochemistry, Geophysics, Geosystems*, **8**: Q08006. doi:10.1029/2006GC001492.
- Shirmohammad, F., Smith, P., Anderson, R., and McNicoll, V. 2011. The Jurassic succession at Lisadee Lake (Tulsequah map area, British Columbia, Canada) and its bearing on the tectonic evolution of the Stikine terrane. *Volumina Jurassica*, **9**: 43–60.
- Simard, R.-L. 2003. Geological map of southern Semenof Hills (part of NTS 105E/1,7,8), south-central Yukon (1:50 000 scale). Yukon Geological Survey, Open File 2003-12.
- Souther, J.G. 1977. Volcanism and tectonic environments in the Canadian Cordillera: a second look. Special Paper - Geological Association of Canada, no. 16, pp. 3–24.
- Souther, J.G. 1991. Volcanic regimes, Chapter 14. In *Geology of the Cordilleran orogen in Canada*. Edited by H. Gabrielse and C.J. Yorath. Geological Survey of Canada, *Geology of Canada*, **4**, pp. 457–490.
- Struik, L.C., Schiarizza, P., Orchard, M.J., Cordey, F., Sano, H., MacIntyre, D.G., et al. 2001. Imbricate architecture of the upper Paleozoic to Jurassic oceanic Cache Creek Terrane, central British Columbia. *Canadian Journal of Earth Sciences*, **38**(4): 495–514. doi:10.1139/e00-117.
- Sun, S.-s., and McDonough, W.F. 1989. Chemical and isotopic systematics of oceanic basalts: implications for mantle composition and processes. *Geological Society, London, Special Publications*, **42**: 313–345. doi:10.1144/GSL.SP.1989.042.01.19.
- Tardy, M., Lapiere, H., Struik, L.C., Bosch, D., and Brunet, P. 2001. The influence of mantle plume in the genesis of the Cache Creek oceanic igneous rocks: Implications for the geodynamic evolution of the inner accreted terranes of the Canadian Cordillera. *Canadian Journal of Earth Sciences*, **38**(4): 515–534. doi:10.1139/e00-104.
- Tempelman-Kluit, D.J. 1984. *Geology, Laberge (105E) and Carmacks (105I), Yukon Territory*. Geological Survey of Canada, Open File 1101, 1:250 000.
- Tempelman-Kluit, D.J. 2009. *Geology of Carmacks and Laberge map areas, central Yukon*: Incomplete draft manuscript on stratigraphy, structure and its early interpretation (ca. 1986). Geological Survey of Canada, Open File 5982: 399 p.
- Thorstad, L.E. 1977. The Upper Triassic “Kutcho Formation”, Cassiar Mountains, north-central British Columbia. Unpublished Master's thesis, University of British Columbia, Vancouver, British Columbia, 271 p.
- Walker, J.D., Geissman, J.W., Bowring, S.A., and Babcock, L.E. (Compilers). 2012. *Geologic Time Scale v. 4.0*. Geological Society of America.
- Wernicke, B., and Klepacki, D.W. 1988. Escape hypothesis for the Stikine block. *Geology*, **16**: 461–464. doi:10.1130/0091-7613(1988)016<0461:EHFTSB>2.3.CO;2.
- Wheeler, J.O. 1961. Whitehorse map-area, Yukon Territory (105D). Geological Survey of Canada, Memoir, 312: 156 p.
- Wheeler, J.O., and McFeely, P. 1991. Tectonic assemblage map of the Canadian Cordillera and adjacent parts of the United States of America. Geological Survey of Canada, Map 1712A, 1:2 000 000. doi:10.4095/133549.
- White, D., Colpron, M., and Buffett, G. 2012. Seismic and geological constraints on the structure and hydrocarbon potential of the northern Whitehorse trough, Yukon, Canada. *Bulletin of Canadian Petroleum Geology*, **60**: 239–255. doi:10.2113/gscpgbull.60.4.239.
- Winchester, J.A., and Floyd, P.A. 1977. Geochemical discrimination of different magma series and their differentiation products using immobile elements. *Chemical Geology*, **20**: 325–343. doi:10.1016/0009-2541(77)90057-2.
- Wood, D.A. 1980. The application of a Th-Hf-Ta diagram to problems of tectonomagmatic classification and to establishing the nature of crustal contamination of basaltic lavas of the British Tertiary Volcanic Province. *Earth and Planetary Science Letters*, **50**: 11–30. doi:10.1016/0012-821X(80)90116-8.
- Yukon Geological Survey. 2018. Yukon Digital Bedrock Geology. http://www.geology.gov.yk.ca/update_yukon_bedrock_geology_map.html [accessed: July 15, 2018].
- Zagorevski, A. 2016. Geochemical data of the northern Cache Creek and Stikine terranes and their overlap assemblages, British Columbia and Yukon. Geological Survey of Canada Open File, 8039, pp. 1–11. doi:10.4095/299347.
- Zagorevski, A., Corriveau, A.-S., McGoldrick, S., Bédard, J.H., Canil, D., Golding, M.L., et al. 2015. Geological framework of ancient oceanic crust in northwestern British Columbia and southern Yukon – GEM Cordillera 2. Geological Survey of Canada, Open File 7957, 10 p. doi:10.4095/297273.